

Keep the Core: Adversarial Priors for Significance-Preserving Brain MRI Segmentation

Feifei Zhang^{1,2,3}, Zhenhong Jia^{1,2,*}, Sensen Song^{1,2}, Fei Shi^{1,2,3}, Aoxue Chen⁵, Dayong Ren^{4, *}

¹ School of Computer Science and Technology, Xinjiang University, Urumqi, 830046, China,

² Key Laboratory of Signal Detection and Processing, Xinjiang University, Urumqi, 830046, China,

³ Xinjiang Multimodal Intelligent Processing and Information Security Engineering Technology

Research Center, Urumqi, 830046, China,

⁴ National Key Laboratory for Novel Software Technology, Nanjing University, Nanjing 210023, China,

⁵ Department of Neurology, Jiangsu Province Hospital,

The First Affiliated Hospital of Nanjing Medical University, Nanjing 210029, China.

Abstract

Medical image segmentation is constrained by sparse pathological annotations. Existing augmentation strategies, from conventional transforms to random masking for self-supervision, are feature-agnostic: they often corrupt critical diagnostic semantics or fail to prioritize essential features. We introduce "Keep the Core," a novel data-centric paradigm that uses adversarial priors to guide both augmentation and masking in a significance-preserving manner. Our approach uses SAGE (Sparse Adversarial Gated Estimator), an offline module identifying minimal tokens whose micro-perturbation flips segmentation boundaries. SAGE forges the Token Importance Map W by solving an adversarial optimization problem to maximally degrade performance, while an ℓ_1 sparsity penalty encourages a compact set of sensitive tokens. The online KEEP (Key-region Enhancement & Preservation) module uses W for a two-pronged augmentation strategy: (1) Semantic-Preserving Augmentation: High-importance tokens are augmented, but their original pixel values are strictly restored. (2) Guided-Masking Augmentation: Low-importance tokens are selectively masked for an MAE-style reconstruction, forcing the model to learn robust representations from preserved critical features. "Keep the Core" is backbone-agnostic with no inference overhead. Extensive experiments show SAGE's structured priors and KEEP's region-selective mechanism are highly complementary, achieving state-of-the-art segmentation robustness and generalization on 2D medical datasets.

1. Introduction

Medical image segmentation serves as a cornerstone for modern clinical diagnosis, prognostic assessment, and surgical planning [6, 57, 58], providing quantitative morphological and spatial information from CT and MRI for tumor delineation and organ mapping. However, the remarkable performance of these models relies heavily on large-scale, high-quality, pixel-level annotated datasets. In the medical domain, acquiring such data faces two major bottlenecks: (1) Data Scarcity: Privacy regulations, equipment costs, and data silos make acquiring large-scale medical images challenging. (2) Annotation Scarcity: Labeling medical images requires expert radiologists or pathologists, a process that is both time-consuming and expensive. More critically, pathological annotations are often extremely sparse spatially—for instance, micro-nodules, early-stage polyps, or diffuse lesions may occupy less than 1% of an entire scan [21, 46]. To mitigate data scarcity, Data Augmentation (DA) has become a standard component in deep learning training [43]. Traditional DA methods, such as affine transformations (rotation, scaling) and color jittering (brightness, contrast), are vital for improving model robustness to variations in position and illumination.

However, when more advanced regional augmentation methods (e.g., Cutout [11], Random Erasing [60], or even Mixup [59]) are blindly applied to medical images, they often yield catastrophic results. These methods, designed for natural images, assume high information redundancy. In medical images, when a random occlusion patch happens to cover a tiny, critical lesion, the sample's critical diagnostic semantics are entirely destroyed [10]. The model learns from this "corrupted" sample may be noise, artifacts, or an incorrect "background prior." This issue of semantics-

*Corresponding author.

agnostic data manipulation is not limited to traditional DA; it extends directly to modern self-supervised strategies like Masked Image Modeling.

As another solution to annotation scarcity, Self-Supervised Learning (SSL), particularly Masked Image Modeling (MIM) [3] as exemplified by the Masked Autoencoder (MAE) [19] has shown immense potential. Yet, its core augmentation technique—random masking—suffers from the same ‘blind spot’ in medical imaging. In natural images, information is highly redundant (e.g., sky, grass), and random masking forces the model to learn global context. In medical images, a single 16x16 token might contain the entire early-stage lesion. MAE’s random policy has a high probability of masking all critical pathological tokens. This leads to a paradox: the model spends significant pre-training time learning to perfectly reconstruct healthy anatomical structures (i.e., the “background”) but learns little about the critical lesion representations [50]. This strategy is not only inefficient but also creates a fundamental bias between the learned representation and the downstream segmentation task (i.e., localizing the lesion).

These challenges point to a common root: the field lacks a unified, semantics-aware augmentation paradigm. Both conventional transforms and SSL masking operate ‘blindly,’ failing to distinguish ‘critical’ from ‘non-critical’ tokens. We propose a more fundamental and robust definition of “importance.” We argue that: A token’s “importance” is not defined by its visual saliency, but by its “Adversarial Vulnerability” to the model’s decision boundary. In other words, if applying a tiny, imperceptible perturbation to a token can cause the model’s segmentation output (e.g., Dice score) to catastrophically collapse (i.e., “flip the segmentation boundary”), then that token carries the most critical diagnostic information. In medical images, these “vulnerable” tokens correspond precisely to the subtle textures, ambiguous borders, or micro-structures that the model relies on to distinguish “pathology” from “health.” These regions are the true cornerstones of the model’s decision-making and are the most easily destroyed by DA or ignored by MAE. Based on this core insight, we propose “Keep the Core,” a novel data-centric paradigm that leverages adversarial priors to intelligently guide both data augmentation and masked self-supervised learning.

Our approach begins with the SAGE (Sparse Adversarial Gated Estimator), an offline module whose sole objective is to compute this “adversarial vulnerability.” SAGE operates on a token grid, and its core task is to solve a sparse adversarial optimization problem: to find the minimum set of tokens where applying a micro-perturbation is sufficient to “flip” the model’s segmentation boundary. The output of SAGE is a normalized Token Importance Map W , which precisely quantifies each token’s contribution to the model’s decision, thereby effectively localizing the most sensitive

pathological regions.

In the online training stage, the KEEP (Key-region Enhancement & Preservation) module utilizes the offline-generated W map to execute an adaptive, two-pronged intervention on the standard training pipeline (including DA and MAE): 1. Preservation: “Augment-and-Restore” for Critical Tokens For high-importance tokens identified by W (i.e., the “core” lesion areas): we first apply standard intensity and affine transformations (DA) to the entire image. Then, we execute a critical “restore” operation to ensure the integrity and high-fidelity of core semantic features, while still allowing the model to observe the core features in varied augmented contexts. 2. Guided Masking for Non-Critical Tokens. For low-importance tokens in W (e.g., background, healthy tissue): we perform guided MAE-style masking. We prioritize sampling tokens for masking from this “non-critical” pool. This forces the model to solve a more valuable task: “reconstruct the surrounding non-critical context, given the (visible) core pathological features.” This drastically improves representation learning efficiency and forces the model to learn robust representations that rely on the preserved critical features. The “Keep the Core” framework is backbone-agnostic and introduces no inference overhead. We conduct extensive experiments on multiple 2D medical segmentation datasets (e.g., [20, 36]). Our contributions are summarized as follows:

- We introduce adversarial vulnerability as a new definition of feature importance, which is more aligned with the segmentation boundary than visual saliency.
- We propose a two-stage SAGE-KEEP framework where an offline-generated adversarial map (W) guides an online dual-path strategy of semantic preservation and guided masking.

2. Related Work

Our work is positioned at the intersection of network architecture and data-centric learning strategies. We uniquely categorize both traditional Data Augmentation and the masking policies within Self-Supervised Learning as two facets of a broader augmentation paradigm, which our work aims to unify.

2.1. Architectural Evolution

With the rapid progress of deep learning, a significant body of research has focused on improving segmentation performance through architectural innovation. Early CNN-based models such as FCN [32], U-Net [41] and its variants (U-Net++ [62], U-Net3+ [22], nnU-Net [26]) leveraged encoder-decoder architectures with multi-level skip connections to improve multi-scale feature fusion and lesion localization [30], but remained limited by local receptive fields and insufficient global context modeling [2, 38–40, 63]. Transformer-based approaches [14], including TransUNet

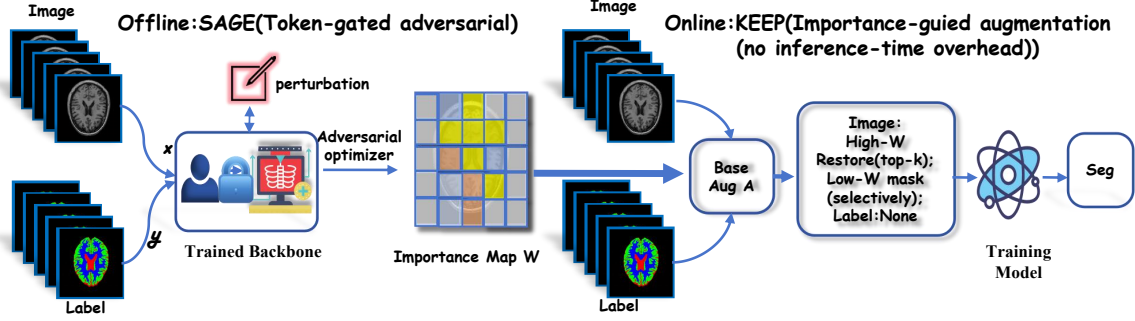


Figure 1. "Keep the Core". **(Left)** The offline SAGE (Sparse Adversarial Gating Evaluator) solves an adversarial optimization problem to generate a Token Importance Map (W). **(Right)** The online KEEP (Key-region Enhancement and Preservation) module leverages W to apply its two-pronged strategy: (1) "Augment-and-Restore" for critical tokens and (2) "Guided Masking" for non-critical tokens.

[8], UTNet [15], ViT-UNet [61], and Swin-UNet [4], introduced self-attention to aggregate global information, yet their quadratic complexity in self-attention incurs substantial computational costs [7, 13, 18, 28, 29, 37, 47, 56]. More recently, state space models (SSMs) [17] such as Mamba have emerged as a promising alternative, offering linear complexity while maintaining strong long-range dependency modeling. Vision Mamba backbones and U-Net variants [31] as well as hybrid designs like LMa-UNet [52], LocalMamba [24], and SegMamba [53] further enhance spatial awareness and multi-scale fusion. While architectural advancements are crucial, our work is complementary and backbone-agnostic. We address a more fundamental challenge: how models learn from limited and sparsely annotated data, regardless of the specific architecture employed.

2.2. DA and Semantics Preservation

Data Augmentation (DA) is a standard technique to combat data scarcity [43]. Simple affine and color transformations are beneficial. However, regional dropout methods, such as Cutout [11] and Random Erasing [60], designed for information-redundant natural images, often fail in medical contexts. As noted by [10], randomly occluding a tiny, critical lesion destroys the sample's diagnostic semantics, forcing the model to learn from corrupted labels. Several works have attempted "semantics-aware" augmentation. For instance, [16] used saliency maps (e.g., [42, 44]) to prevent augmentation in important areas. However, extensive research [1] shows that saliency maps are unreliable. At best, they reflect only *where* a model is looking, not what is *critical* to its decision boundary [27]. Our approach differs by defining importance not via post-hoc attribution, but directly through adversarial vulnerability, which is inherently tied to the decision boundary.

2.3. Masked Image Modeling in Medical Imaging

Masked Image Modeling (MIM), exemplified by the Masked Autoencoder (MAE) [19], has become a powerful self-supervised learning (SSL) strategy. We analyze it here as a modern form of data augmentation, where the core augmentation technique is the "random masking" policy. However, this "random masking" is suboptimal for medical images. Pathological features (e.g., micro-nodules) are often small and sparse. A 75% random masking has a high probability of masking all critical features, forcing the model to spend its capacity learning to reconstruct healthy, "background" anatomy [50]. This creates a bias, where the pre-trained representation is proficient at anatomy but naive about pathology. Some works have explored guided masking, but often rely on saliency or visual features. Our SAGE module provides a more robust, non-random prior, guiding the MAE task to focus on reconstructing the *context* around the critical features we explicitly preserve.

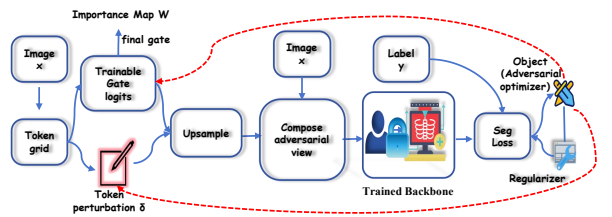


Figure 2. **The Offline SAGE Module.** SAGE freezes the segmentation network and optimizes a learnable Gated Mask m and a Perturbation δ . By minimizing the combined adversarial and sparsity objective, it forces the mask to converge on the most sensitive pathological regions, producing the Token Importance Map W .

3. Method

3.1. Overview

We introduce **Keep the Core**, a novel framework designed to reconcile the conflict between data scarcity and semantic integrity in medical image segmentation. As illustrated in Fig. 1, our framework decouples the process into two distinct yet complementary phases: (1) **Offline Vulnerability Assessment (SAGE)**: Before the main training loop, we perform a computationally intensive “stress test” on the training data. By solving a sparse adversarial optimization problem, the SAGE module identifies the minimal set of image tokens—termed the “Core”—that are most critical for the model’s decision boundary. (2) **Online Robustness Enhancement (KEEP)**: During the efficient online training phase, the KEEP module utilizes these pre-computed importance priors to execute a meta-augmentation paradigm. It does not replace standard augmentations, but intelligently guides them by selectively protecting the fragile core tokens while aggressively challenging the non-critical context, achieving a balance between feature preservation and robustness without inference-time overhead.

3.2. SAGE: Sparse Adversarial Gating Evaluator

The primary objective of SAGE is to generate a pixel-level *Token Importance Map* W for each training sample (x, y) . Unlike heuristic saliency methods (e.g., Grad-CAM) which only reflect where the model “looks,” SAGE actively “probes” the model to find where it is “vulnerable.” We hypothesize that the most critical diagnostic features are those whose perturbation leads to the most significant collapse in segmentation performance.

3.2.1. Adversarial Gating Formulation

As depicted in Fig. 2, SAGE operates on a frozen, pre-trained segmentation oracle $f(\cdot)$. Given an input image $x \in \mathbb{R}^{H \times W}$, we discretize the spatial domain into a grid of tokens with resolution (H_t, W_t) . To locate critical tokens, we introduce two learnable tensor components:

- **Latent Gate** $G \in \mathbb{R}^{H_t \times W_t}$: A real-valued parameter map that controls the spatial selection of tokens.
- **Perturbation** $\delta \in \mathbb{R}^{C \times H_t \times W_t}$: A learnable noise tensor bounded by an ℓ_∞ norm constraint $\|\delta\|_\infty \leq \epsilon$.

To enable gradient-based optimization of the discrete selection process, we employ a differentiable relaxation using temperature annealing. The binary-like mask m is computed as $m = \sigma(G/T)$, where $\sigma(\cdot)$ is the sigmoid function and T is a temperature scalar that decays over time. The resulting adversarial sample x_{adv} is synthesized by injecting the perturbation only into the gated tokens:

$$x_{\text{adv}} = \text{clamp}(x + \mathcal{U}(m) \odot \mathcal{U}(\delta)), \quad (1)$$

where $\mathcal{U}(\cdot)$ denotes nearest-neighbor upsampling to match

Algorithm 1 SAGE: Offline Importance Generation

Input: Image x , Label y , Frozen Oracle $f(\cdot)$.
Params: Budget ϵ , Temp $T_{\text{start}} \rightarrow T_{\text{end}}$, Steps N .
Output: Token Importance Map W .

```

1: Initialize  $G \leftarrow \mathbf{0}$ ,  $\delta \leftarrow \mathbf{0}$ .
2: for  $step = 1$  to  $N$  do
3:    $T \leftarrow \text{Anneal}(T_{\text{start}}, T_{\text{end}}, step)$ 
4:    $m \leftarrow \sigma(G/T)$                                  $\triangleright$  Generate soft mask
5:    $x_{\text{adv}} \leftarrow \text{clamp}(x + \mathcal{U}(m) \odot \mathcal{U}(\delta))$ 
6:    $\mathcal{L} \leftarrow -\mathcal{L}_{\text{seg}}(f(x_{\text{adv}}), y) + \mu\|m\|_1 + \beta\|\delta\|_1$ 
7:   Update  $G, \delta$  via Adam to minimize  $\mathcal{L}$ 
8:    $\delta \leftarrow \text{clip}(\delta, -\epsilon, \epsilon)$                    $\triangleright$  Enforce budget
9: end for
10: return  $W \leftarrow \sigma(G/T_{\text{end}})$ 

```

the image resolution, and \odot represents the Hadamard product.

3.2.2. Sparse Optimization Objective

SAGE formulates importance discovery as a *Min-Max* optimization game. We seek to maximize the segmentation error (attack) while simultaneously minimizing the area of the selected tokens (sparsity). This ensures that W captures only the *minimal sufficient* features required to flip the prediction. The total objective $\mathcal{L}_{\text{SAGE}}$ is defined as:

$$\mathcal{L}_{\text{attack}} = \lambda_{\text{ce}} \mathcal{L}_{\text{CE}}(f(x_{\text{adv}}), y) + \lambda_{\text{dice}} \mathcal{L}_{\text{Dice}}(f(x_{\text{adv}}), y), \quad (2)$$

$$\mathcal{L}_{\text{sparse}} = \mu_{\text{sparse}} \|m\|_1 + \beta_{\delta} \|\delta\|_1, \quad (3)$$

$$\min_{G, \delta} \mathcal{L}_{\text{SAGE}} = \min_{G, \delta} (-\mathcal{L}_{\text{attack}} + \mathcal{L}_{\text{sparse}}). \quad (4)$$

Here, the ℓ_1 penalty on m is crucial: it forces the gate to “shut down” for all pixels except those strictly necessary to degrade the model’s performance. As shown in Algorithm 1, we iteratively update G and δ . Upon convergence, the final Importance Map is derived as $W = \sigma(G/T_{\text{end}})$, effectively highlighting the “Achilles’ heel” of the input sample.

3.3. KEEP: Key-region Enhancement and Preservation

The KEEP module operationalizes our unified augmentation paradigm. It functions as an intelligent wrapper around the standard data augmentation pipeline $\mathcal{A}(\cdot)$. As illustrated in Fig. 3 and formalized in Algorithm 2, it follows a “Protect-and-Challenge” philosophy: safeguarding high-value pathological semantics while forcing the model to infer context from incomplete data.

After a standard stochastic augmentation $\mathcal{A}(\cdot)$ (e.g., random intensity shifts, blurring) is applied to produce x_{aug} , KEEP applies the following two interventions:

Algorithm 2 KEEP: Online Guided Augmentation

Input: Image x , Importance Map W , Standard Augmentor \mathcal{A} .
Params: Top-K value K , Optional mask threshold τ_{low} . **Output:** Final augmented image x_{final} .

```

1:  $x_{aug} \leftarrow \mathcal{A}(x)$             $\triangleright$  Apply standard DA (e.g., affine, color)
2:  $S_{local} \leftarrow \text{Pool}(W)$   $\triangleright$  Compute token-level importance scores
3:
4: // Path 1: Preserve Critical Core (Fig. 3 Top)
5:  $M_{core} \leftarrow \text{TopK\_Mask}(S_{local}, K)$        $\triangleright$  Get mask for Top-K tokens
6:  $x' \leftarrow x_{aug} \odot (1 - M_{core}) + x \odot M_{core}$   $\triangleright$  Restore original pixels
7:
8: // Path 2: Optional Guided Masking (Fig. 3 Bottom)
9:  $M_{mask} \leftarrow 0$ 
10: if  $\tau_{low} > 0$  then            $\triangleright$  Masking is optional
11:    $M_{potential} \leftarrow \mathbb{I}(S_{local} < \tau_{low})$   $\triangleright$  Find low-score tokens
12:    $M_{mask} \leftarrow \text{SampleSubset}(M_{potential})$   $\triangleright$  Sample from non-critical pool
13: end if
14:  $x_{final} \leftarrow x' \odot (1 - M_{mask})$   $\triangleright$  Apply mask (or identity if  $M_{mask}$  is 0)
15: return  $x_{final}$ 

```

3.3.1. Core Preservation (Augment-and-Restore)

Standard augmentations can inadvertently destroy subtle pathological details (e.g., washing out the texture of a micro-nodule). To prevent this, we identify the set of Top-K tokens M_{core} with the highest importance scores (derived from W). As shown in the upper branch of Fig. 3, we strictly *restore* the original pixel values from the pre-augmentation image x within these tokens:

$$x' = x_{aug} \odot (1 - M_{core}) + x \odot M_{core}. \quad (5)$$

This "Augment-and-Restore" strategy ensures that the model always sees high-fidelity data for the most diagnostically relevant features, while the surrounding context remains augmented to provide variability.

3.3.2. Optional Guided Context Masking

Conversely, medical background tokens are often highly redundant. To prevent the model from relying on trivial correlations and to enhance representation learning, we optionally employ a guided masking strategy. We identify a pool of non-critical tokens $M_{potential}$ (e.g., those with importance scores below a threshold τ_{low}). As shown in the lower branch of Fig. 3, we randomly sample a subset M_{mask} from this pool and mask them (e.g., set to zero or a fill value):

$$x_{final} = x' \odot (1 - M_{mask}). \quad (6)$$

This effectively constructs a hard reconstruction task, compelling the network to learn robust global representations by inferring the missing context solely from the preserved core features. If this optional step is skipped, $x_{final} = x'$.

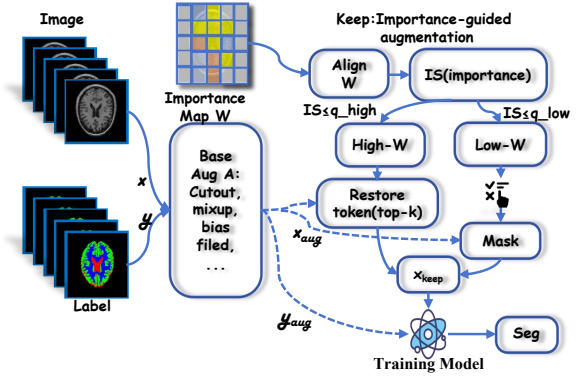


Figure 3. **The Online KEEP Module.** Using the Importance Map W , KEEP performs a two-step intervention after standard augmentation. **Path 1 (Top):** Critical tokens (Red) are restored to their original values to prevent semantic corruption. **Path 2 (Bottom):** Non-critical background tokens (Blue) are optionally masked to encourage robust global context learning.

4. Experiments

4.1. Experimental Setup

Datasets. We validate our framework on two public benchmarks covering 2D visual modality:

- **OASIS-1** [34]: Derived from the Open Access Series of Imaging Studies, this dataset comprises T1-weighted MRI scans from 421 subjects (aged 18–96). The images were acquired with a resolution of 176×208 pixels and a slice thickness of 1.25 mm (TR=9.7 ms, TE=4.0 ms, TI=20 ms). Following standard protocols, we utilize the provided manual segmentation masks for Cerebrospinal Fluid (CSF), Grey Matter (GM), and White Matter (WM).
- **MRBrainS13** [35]: From the MICCAI 2013 challenge, this dataset contains multi-sequence scans of 20 subjects acquired on a 3.0T Philips Achieva scanner. It provides T1 (TR: 7.9 ms, TE: 4.5 ms), T1-IR, and T2-FLAIR sequences. All scans are co-registered and bias-corrected with a voxel spacing of $0.96 \times 0.96 \times 3.00$ mm. We utilize the provided labels for CSF, GM, and WM segmentation.

Implementation Details. Our framework is implemented in PyTorch and trained on a single NVIDIA A100 GPU (40GB). We employ the AdamW optimizer with an initial learning rate of 1×10^{-3} and a cosine annealing decay schedule. The batch size is set to 16. Models are trained for 50 epochs on OASIS-1 and 200 epochs on MRBrainS13 to ensure convergence. For evaluation, we employ an early-stopping strategy where the checkpoint achieving the highest Dice score on the validation set is selected.

Hyperparameters: Following [12, 54], the annealing parameter α in SAGE is linearly increased from $\alpha_{init} = 0.1$ to $\alpha_{end} = 10$

to encourage binary mask convergence. The temperature parameter τ is set to 0.6 across all experiments. Crucially, these hyperparameters are fixed across different backbones, demonstrating the robust and plug-and-play nature of our framework.

Baseline Methods. To ensure a rigorous comparison, we benchmark *Keep the Core* against a comprehensive suite of augmentation strategies across three representative backbones: UNet, SwinUNet [4], and SwinUMamba [31]. The comparison methods are categorized into: (1) **Pixel-level Augmentation**: Gaussian noise [51], Gaussian blur [25], Gamma correction [49], Brightness/Contrast adjustment [45], and Bias field perturbation [5]. (2) **Token-level Augmentation**: Random Erasing [60], Cutout [11], Mixup [59], Cutmix [55], HSMix [48], MRS [23], and ABD [9]. All baselines are re-implemented using their officially reported optimal configurations. To guarantee a fair and rigorous comparison, all models (baselines and ours) are trained from scratch using an identical optimization protocol, data splits, and hyperparameter settings, thereby isolating the performance contribution of the augmentation strategy.

4.2. Results on OASIS-1 and MRBrainS13 Datasets

We conduct a comprehensive evaluation of our "Keep the Core" (KC) framework on two medical image segmentation benchmarks: OASIS-1 and MRBrainS13. As shown in Table 1 and Table 2, we systematically compare standard data augmentation methods against their corresponding "Keep the Core" enhanced versions across three representative backbones: UNet, SwinUNet, and SwinUMamba. From the results, it is observed that while original data augmentation techniques contribute to performance improvements, our proposed "Keep the Core" framework further enhances the efficacy of these SOTA augmentation approaches. Specifically, the KC framework yields substantial performance gains across nearly all augmentation methods. This is visually evident in both tables, where the red up-arrows (\uparrow) for improvements overwhelmingly outnumber the rare green down-arrows (\downarrow) for metric degradations. On the relatively simpler OASIS-1 dataset (Table 1), the "Keep the Core" framework demonstrates stable improvements. For instance, with the UNet backbone, KC-Gaussian Noise improves the Dice score by 0.39% (CSF) and 0.23% (GM) and reduces the HD95 distance by 0.0433mm (CSF) and 0.032mm (GM) compared to the standard Gaussian Noise. On the more advanced SwinUMamba backbone, the KC-ABD method maintains improvements on major metrics with only slight fluctuations in sub-metrics, highlighting the framework's robustness. The performance gains are particularly significant on the more challenging MRBrainS13 dataset (Table 2). Notably, on the SwinUMamba backbone, the KC-MRS method achieves an absolute Dice score improvement of 1.60% (CSF) and 1.39%

(GM), while reducing HD95 distance by 0.2454mm (CSF) and 0.8471mm (GM), and ASD by 0.0609mm (CSF) and 1.1584mm (WM). These results indicate our framework's strong adaptability in complex medical imaging scenarios. It is worth noting that our framework's effectiveness is particularly pronounced for information-deleting augmentations (e.g., Cutout, Random Erasing) and mixing-based augmentations (e.g., Mixup, Cutmix). These methods are prone to introducing perturbations, and the significance-preserving mechanism of "Keep the Core" effectively mitigates this issue, leading to sub-gains in overall performance.

Cross-Architecture Consistency Our method demonstrates good compatibility across different network architectures. For the relatively simple UNet architecture, the framework provides stable performance gains. The improvements are more pronounced for the Transformer-based SwinUNet. On the state-of-the-art SwinUMamba architecture, the framework still delivers significant benefits. This indicates our method is not limited to a specific architecture and possesses broad applicability. Furthermore, the extent of improvement is influenced by the architectural choice. Compared to simpler CNN architectures, modern architectures with stronger representation capabilities, such as SwinUMamba, can better leverage the saliency priors provided by our framework, thus achieving greater performance enhancements.

Extended Experimental Results & Qualitative Evaluation Tables 1 and 2 in the main paper present the core comparative results. To provide a more exhaustive validation, we include extensive supplementary tables in the Appendix (e.g., Tables 5-10). These tables expand upon our main findings, providing a granular breakdown of the systematic comparisons for all 12 augmentation methods across every backbone and metric. This comprehensive dataset serves to rigorously substantiate the effectiveness and robustness of our proposed "Keep the Core" framework. In addition, the corresponding qualitative results are included in the Supplementary Material and are referenced as Fig. 7 and Fig. 8.

4.3. Ablation Study

4.3.1. Robustness Evaluation of Importance Maps

We conduct a systematic comparison of the effects of importance maps on the MRBrainS13 dataset. Specifically, we first use one segmentation model to generate importance maps, and then combine these maps with different data augmentation strategies to train another model, thereby evaluating the robustness of the importance-map generation module in a cross-model setting. As shown in Tables 3 and 4, when using the importance maps generated by SwinUNet [4], denoted as Keep the Core (SwinUNet Map), to

Table 1. Comprehensive evaluation on OASIS-1 dataset. 'Keep the Core' (KC) methods are compared to their non-KC counterparts(e.g., KC-Gaussian vs. Gaussian Noise). Metric improvements are marked with a top-right red arrow (\uparrow), degradations with a bottom-right green arrow (\downarrow).

Backbone	Augmentation	Dice \uparrow			HD95(mm) \downarrow			ASD(mm) \downarrow			IOU \uparrow		
		CSF	GM	WM	CSF	GM	WM	CSF	GM	WM	CSF	GM	WM
UNet	Baseline	0.9062	0.9134	0.9181	1.1267	1.2138	2.0824	0.2581	0.3611	0.6198	0.8442	0.8599	0.8688
	Gaussian Noise	0.9038	0.9141	0.9227	1.1452	1.1815	1.9931	0.2588	0.3466	0.5883	0.8403	0.8613	0.8748
	Keep the Core-Gaussian Noise	0.9077 \uparrow	0.9164 \uparrow	0.9228 \uparrow	1.1019 \uparrow	1.1495 \uparrow	2.0568 \downarrow	0.2571 \uparrow	0.3462 \uparrow	0.5788 \uparrow	0.8463 \uparrow	0.8643 \uparrow	0.8749 \uparrow
	Cutout	0.9081	0.9132	0.9212	1.1342	1.2213	2.1083	0.2667	0.3675	0.6290	0.8472	0.8594	0.8719
SwinUNet	Keep the Core-Cutout	0.9099 \uparrow	0.9135 \uparrow	0.9293 \uparrow	1.1006 \uparrow	1.1940 \uparrow	1.9644 \uparrow	0.2624 \uparrow	0.3618 \uparrow	0.5620 \uparrow	0.8498 \uparrow	0.8596 \uparrow	0.8797 \uparrow
	Baseline	0.9051	0.9145	0.9226	1.1233	1.1778	1.7979	0.2966	0.3501	0.5340	0.8425	0.8619	0.8743
	Random Erasing	0.8989	0.9085	0.9150	1.1831	1.2965	2.1528	0.3351	0.3998	0.6200	0.8316	0.8516	0.8622
	Keep the Core-Random Erasing	0.9033 \uparrow	0.9124 \uparrow	0.9193 \uparrow	1.1349 \uparrow	1.2193 \uparrow	1.9367 \uparrow	0.3033 \uparrow	0.3756 \uparrow	0.5915 \uparrow	0.8388 \uparrow	0.8580 \uparrow	0.8692 \uparrow
SwinUMamba	Cutmix	0.9097	0.9182	0.9258	1.1309	1.1685	1.6913	0.2755	0.3299	0.4516	0.8513	0.8688	0.8796
	Keep the Core-Cutmix	0.9113 \uparrow	0.9187 \uparrow	0.9230 \downarrow	1.1297 \uparrow	1.1683 \uparrow	1.6910 \uparrow	0.2748 \uparrow	0.3188 \uparrow	0.4512 \uparrow	0.8517 \uparrow	0.8691 \uparrow	0.8798 \uparrow
	Baseline	0.9207	0.9261	0.9336	1.0219	1.0675	1.5723	0.1999	0.2471	0.3405	0.8688	0.8822	0.8938
	ABD	0.9233	0.9276	0.9362	1.0215	1.0591	1.5057	0.1997	0.2450	0.3426	0.8731	0.8843	0.8972
SwinUMamba	Keep the Core-ABD	0.9234 \uparrow	0.9273 \downarrow	0.9363 \uparrow	1.0218 \downarrow	1.0590 \uparrow	1.4861 \uparrow	0.1996 \uparrow	0.2449 \uparrow	0.3352 \uparrow	0.8739 \uparrow	0.8846 \uparrow	0.8976 \uparrow
	Mixup	0.9223	0.9310	0.9367	1.0480	1.1090	1.6076	0.1966	0.2346	0.3553	0.8727	0.8908	0.9000
	Keep the Core-Mixup	0.9228 \uparrow	0.9314 \uparrow	0.9369 \uparrow	1.0479 \uparrow	1.1079 \uparrow	1.6070 \uparrow	0.1965 \uparrow	0.2342 \uparrow	0.3530 \uparrow	0.8730 \uparrow	0.8996 \uparrow	0.9040 \uparrow

Table 2. Comprehensive evaluation on MRBrainS13 dataset. 'Keep the Core' (KC) methods are compared to their non-KC counterparts (e.g., KC-Gamma vs. Gamma Correction). Metric improvements are marked with a top-right red arrow (\uparrow), degradations with a bottom-right green arrow (\downarrow).

Backbone	Augmentation	Dice \uparrow			HD95(mm) \downarrow			ASD(mm) \downarrow			IOU \uparrow		
		CSF	GM	WM	CSF	GM	WM	CSF	GM	WM	CSF	GM	WM
UNet	Baseline	0.6947	0.7104	0.7309	1.9670	2.5323	4.7501	0.4383	0.6621	2.0734	0.6115	0.6367	0.6637
	Gamma Correction	0.7034	0.7213	0.7409	1.6832	1.5088	3.6378	0.4286	0.4021	1.3495	0.6237	0.6508	0.6734
	Keep the Core-Gamma	0.7039 \uparrow	0.7198 \downarrow	0.7414 \uparrow	1.6382 \uparrow	1.6529 \downarrow	3.6220 \uparrow	0.4188 \uparrow	0.4252 \downarrow	1.2716 \uparrow	0.6244 \uparrow	0.6593 \uparrow	0.6737 \uparrow
	Brightness/Contrast	0.7028	0.7210	0.7445	1.7027	1.6027	3.7314	0.4118	0.4021	1.5862	0.6228	0.6507	0.6761
SwinUNet	Keep the Core-Brightness/Contrast	0.7075 \uparrow	0.7260 \uparrow	0.7414 \downarrow	1.6739 \uparrow	1.5791 \uparrow	3.0973 \uparrow	0.4102 \uparrow	0.3646 \uparrow	1.0075 \uparrow	0.6211 \downarrow	0.6537 \uparrow	0.6786 \uparrow
	Baseline	0.6659	0.6936	0.7098	2.3639	3.4329	5.2567	0.5767	0.9310	2.1417	0.5710	0.6151	0.6341
	Gaussian Blur	0.6639	0.6928	0.7001	2.3789	3.0653	7.2002	0.6090	0.7770	3.4630	0.5671	0.6100	0.6215
	Keep the Core-Gaussian Blur	0.6639	0.6936 \uparrow	0.7043 \uparrow	2.3546 \uparrow	3.0597 \uparrow	7.0595 \uparrow	0.6025 \uparrow	0.7765 \uparrow	2.7829 \uparrow	0.5669 \downarrow	0.6101 \uparrow	0.6237 \uparrow
SwinUMamba	HSMix	0.6640	0.6917	0.6903	2.5743	3.4378	4.9869	0.6158	1.0094	1.9139	0.5671	0.6087	0.6171
	Keep the Core-HSMix	0.6787 \uparrow	0.7063 \uparrow	0.7095 \uparrow	2.1474 \uparrow	1.6678 \uparrow	4.1721 \uparrow	0.5020 \uparrow	0.7576 \uparrow	1.1763 \uparrow	0.5870 \uparrow	0.6282 \uparrow	0.6350 \uparrow
	Baseline	0.6855	0.7007	0.7017	1.9931	3.1604	7.2391	0.5097	0.9757	2.9280	0.5971	0.6211	0.6226
	MRS	0.6864	0.7068	0.7103	2.0022	2.4285	5.0634	0.4859	0.6938	1.8649	0.5981	0.6312	0.6368
SwinUMamba	Keep the Core-MRS	0.7024 \uparrow	0.7207 \uparrow	0.7249 \uparrow	1.7568 \uparrow	1.5814 \uparrow	3.3757 \uparrow	0.4250 \uparrow	0.4365 \uparrow	0.7065 \uparrow	0.6218 \uparrow	0.6499 \uparrow	0.6556 \uparrow
	Bias Field	0.6844	0.6995	0.7233	2.0534	3.1019	5.2166	0.5317	0.8232	1.9217	0.5956	0.6218	0.6465
	Keep the Core-Bias Field	0.7034 \uparrow	0.7214 \uparrow	0.7525 \uparrow	1.6955 \uparrow	1.5451 \uparrow	3.7876 \uparrow	0.4291 \uparrow	0.3981 \uparrow	1.1525 \uparrow	0.6234 \uparrow	0.6510 \uparrow	0.6780 \uparrow

Table 3. We evaluate the effectiveness of various data augmentation methods on the MRBrainS13 dataset using importance maps generated by different models. The best-performing metrics in the table are highlighted in bold.

Model	Dice \uparrow			HD95(mm) \downarrow			ASD(mm) \downarrow			IOU \uparrow		
	CSF	GM	WM	CSF	GM	WM	CSF	GM	WM	CSF	GM	WM
SwinUMamba	0.6855	0.7007	0.7017	1.9931	3.1604	7.2391	0.5097	0.9757	2.9280	0.5971	0.6211	0.6226
Random Erasing	0.6846	0.7023	0.6997	1.9876	3.0935	6.9380	0.5129	0.9197	3.1028	0.5960	0.6237	0.6239
Keep the core-RandomErasing	0.6999	0.7163	0.7392	1.7354	3.6958	3.9024	0.4512	0.4439	1.3344	0.6180	0.6425	0.6624
Keep the core(SwinUNet Map)-RandomErasing	0.6826	0.6960	0.7076	2.0298	2.5886	5.8871	0.5372	0.7075	2.1070	0.5927	0.6136	0.6290
Cutout	0.6795	0.7000	0.6932	2.1639	3.2561	7.2707	0.5518	1.0129	3.0569	0.5890	0.6204	0.6124
Keep the core-Cutout	0.7024	0.7183	0.7369	1.6590	1.6520	3.7483	0.4404	0.4769	1.1730	0.6218	0.6456	0.6597
Keep the core(SwinUNet Map)-Cutout	0.6889	0.7097	0.7270	1.8591	3.3772	4.2354	0.4929	0.6573	1.6750	0.6015	0.6327	0.6525
Mixup	0.6913	0.7090	0.7126	1.8336	2.2244	3.6060	0.5090	0.6094	1.0710	0.6049	0.6316	0.6349
Keep the core-Mixup	0.7033	0.7199	0.7353	1.8056	1.6822	3.8079	0.4312	0.3883	1.0967	0.6230	0.6486	0.6632
Keep the core(SwinUNet Map)-Mixup	0.6940	0.7093	0.7275	2.0007	2.1704	5.4621	0.5174	0.7329	2.0954	0.5954	0.6241	0.6414
Cutmix	0.6808	0.6910	0.7042	2.0764	3.4679	7.3949	0.5312	0.9627	2.7047	0.5925	0.6074	0.6237
Keep the core-Cutmix	0.6967	0.7130	0.7121	1.9184	2.8017	4.0857	0.4494	0.7503	1.0156	0.6136	0.6398	0.6432
Keep the core(SwinUNet Map)-Cutmix	0.6875	0.7047	0.7311	1.8900	2.0761	4.6900	0.5351	0.5630	1.7522	0.5960	0.6254	0.6506

guide data augmentation for SwinUMamba [31], the overall performance is slightly lower than that obtained when using importance maps generated by SwinUMamba itself. Nevertheless, the performance improvement remains stable and significant. These results provide strong additional evidence for the robustness and effectiveness of our proposed

offline importance-map generation module, SAGE.

4.3.2. Feature Discriminability Analysis

To intuitively validate our method's efficacy, we visualize the feature space using t-SNE in Fig. 4 and Fig. 5. The results are definitive. Qualitatively, features from base-

Table 4. We evaluate the effectiveness of various data augmentation methods on the MRBrainS13 dataset using importance maps generated by different models. The best-performing metrics in the table are highlighted in bold.

Model	Acc \uparrow			Pre \uparrow			Sen \uparrow			Spe \uparrow		
	CSF	GM	WM									
SwinU-Mamba	0.7949	0.7912	0.9159	0.6870	0.6854	0.7483	0.6877	0.7215	0.6981	0.8031	0.7986	0.9222
Random Erasing	0.7949	0.7916	0.9163	0.6904	0.6917	0.7341	0.6825	0.7187	0.7069	0.8035	0.7992	0.9212
Keep the core-RandomErasing	0.7966	0.7941	0.8967	0.6890	0.7107	0.7807	0.7129	0.7236	0.7185	0.8027	0.8017	0.9023
Keep the core(SwinU-Net Map)-RandomErasing	0.7951	0.7919	0.9157	0.6877	0.6947	0.7489	0.7012	0.7019	0.7022	0.8011	0.7996	0.9219
Cutout	0.7940	0.7908	0.9158	0.6811	0.6818	0.7441	0.6839	0.7254	0.6946	0.8027	0.7977	0.9219
Keep the core-Cutout	0.7971	0.7944	0.8865	0.6970	0.7069	0.7954	0.7093	0.7317	0.7036	0.8036	0.8011	0.8922
Keep the core(SwinU-Net Map)-Cutout	0.7956	0.7928	0.8961	0.6933	0.6990	0.7420	0.6809	0.7236	0.7247	0.8044	0.8000	0.9006
Mixup	0.7956	0.7930	0.8752	0.6869	0.6993	0.7488	0.6977	0.7217	0.6922	0.8031	0.8003	0.8809
Keep the core-Mixup	0.7972	0.7952	0.8868	0.6935	0.7193	0.7695	0.7150	0.7218	0.7190	0.8032	0.8028	0.8915
Keep the core(SwinU-Net Map)-Mixup	0.7957	0.7931	0.9165	0.6803	0.6946	0.7616	0.6937	0.7152	0.7151	0.8023	0.7994	0.9222
Cutmix	0.7947	0.7901	0.9155	0.6819	0.6949	0.7283	0.6863	0.6969	0.7050	0.8027	0.7995	0.9211
Keep the core-Cutmix	0.7966	0.7936	0.8653	0.7009	0.7000	0.7496	0.6961	0.7309	0.7097	0.8041	0.8005	0.8695
Keep the core(SwinU-Net Map)-Cutmix	0.7948	0.7927	0.9062	0.6800	0.6996	0.7606	0.6944	0.7123	0.7161	0.8024	0.8000	0.9123

line augmentations (e.g., Cutout, ABD) exhibit significant scattering and inter-class overlap. In contrast, our "Keep the Core" variants (Ours + Aug) produce visibly tighter, more compact, and well-defined clusters. This observation is quantitatively confirmed by the substantial improvements in both the Dunn Index (DI \uparrow) and Silhouette (S \uparrow , [-1, 1]) scores across both datasets. For instance, on OASIS-1, our method boosts the DI for Cutout from 0.2843 to a stark 0.4790. This convergence of visual and metric evidence strongly demonstrates that our framework learns more discriminative representations, successfully minimizing intra-class variance while maximizing inter-class variance. Furthermore, Class Activation Map (CAM) visualizations are provided in the supplementary material (see Fig. 9 and Fig. 10).

4.3.3. The Effect of Parameters

To more comprehensively evaluate the effects of different perturbation magnitudes and the hyperparameter τ on the importance maps, we conduct ablation experiments on the MRBrainS3 dataset, as summarized in Fig. 6. We first combine importance maps generated under different perturbation strengths with multiple data augmentation strategies for testing. As shown in Fig. 6 (a), when the perturbation δ is set to 0.05, the highest average Dice score is achieved consistently across all three augmentation strategies. In addition, Fig. 6 (b) shows that Keep the Core attains its best performance when $\tau = 60\%$. Intuitively, a larger τ means that the restored regions retain information with higher importance scores. However, an excessively large τ reduces the effective sample space, thereby limiting the diversity of augmented data and increasing the sampling cost.

5. Conclusion

In this work, we addressed the feature-agnostic nature of existing augmentation strategies, which often corrupt critical semantics in sparse medical annotations. We pro-

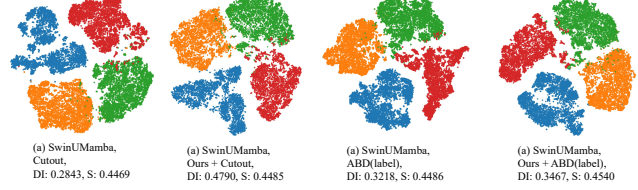


Figure 4. Visualization of deep features on OASIS-1 using t-SNE algorithm [33]. Each color denotes a class. DI: Dunn index(\uparrow). S: Silhouette(\uparrow , [-1, 1]).

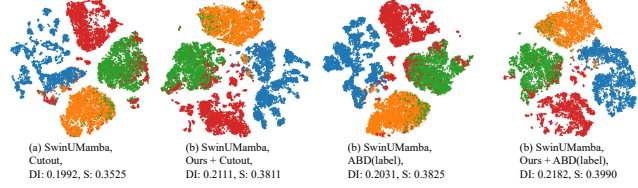


Figure 5. Visualization of deep features on MRBrainS13 using t-SNE algorithm [33]. Each color denotes a class. DI: Dunn index(\uparrow). S: Silhouette(\uparrow , [-1, 1]).

posed "Keep the Core," a novel, data-centric paradigm that redefines feature importance using adversarial vulnerability rather than visual saliency. Our framework introduces SAGE, an offline module that solves a sparse adversarial optimization to identify a minimal set of decision-critical tokens, producing an Importance Map (W). This map guides the online KEEP module, which implements a dual-path strategy: (1) "Augment-and-Restore" to strictly preserve high-importance tokens from augmentation-induced corruption, and (2) "Guided Masking" to selectively challenge the model on low-importance tokens. This SAGE-KEEP pipeline effectively unifies and enhances both conventional DA and masked-image modeling. Extensive experiments demonstrate that our backbone-agnostic approach achieves state-of-the-art robustness and generalization on 2D medical segmentation tasks, validating the clear superiority of

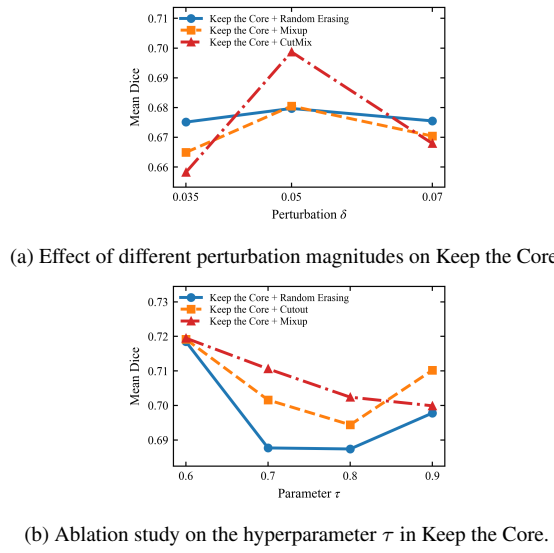


Figure 6. Ablation Study on Parameter Effectiveness.

our significance-preserving paradigm.

Acknowledgments

This work was supported by National Natural Science Foundation of China (No.62261053), Tianshan Talent Training Project - Xinjiang Science and Technology Innovation Team Program (2023TSYCTD0012) and Tianshan Innovation Team Program of Xinjiang Uygur Autonomous Region of China (2023D14012).

References

[1] Julius Adebayo, Justin Gilmer, Michael Muelly, Ian Goodfellow, Moritz Hardt, and Been Kim. Sanity checks for saliency maps. In *Advances in Neural Information Processing Systems (NeurIPS)*, 2018. 3

[2] Reza Azad, Ehsan Khodapanah Aghdam, Amelie Rauland, Yiwei Jia, Atlas Haddadi Avval, Afshin Bozorgpour, Sanaz Karimijafarbigloo, Joseph Paul Cohen, Ehsan Adeli, and Dorit Merhof. Medical image segmentation review: The success of u-net. *IEEE Transactions on Pattern Analysis and Machine Intelligence*, 2024. 2

[3] Hangbo Bao, Li Dong, Songhao Piao, and Furu Wei. Beit: Bert pre-training of image transformers. In *International Conference on Learning Representations (ICLR)*, 2021. 2

[4] Hu Cao, Yueyue Wang, Joy Chen, Dongsheng Jiang, Xiaopeng Zhang, Qi Tian, and Manning Wang. Swin-unet: Unet-like pure transformer for medical image segmentation. In *European conference on computer vision*, pages 205–218. Springer, 2022. 3, 6

[5] Chen Chen, Chen Qin, Huaqi Qiu, Cheng Ouyang, Shuo Wang, Liang Chen, Giacomo Tarroni, Wenjia Bai, and Daniel Rueckert. Realistic adversarial data augmentation for mr image segmentation. In *International Conference on Medical Image Computing and Computer-Assisted Intervention*, pages 667–677. Springer, 2020. 6

[6] Cheng Chen, Juzheng Miao, Dufan Wu, Aoxiao Zhong, Zhiling Yan, Sekeun Kim, Jiang Hu, Zhengliang Liu, Lichao Sun, Xiang Li, et al. Ma-sam: Modality-agnostic sam adaptation for 3d medical image segmentation. *Medical Image Analysis*, 98:103310, 2024. 1

[7] Chen Chen, Yisen Wang, Honghua Chen, Xuefeng Yan, Dayong Ren, Yanwen Guo, Haoran Xie, Fu Lee Wang, and Mingqiang Wei. Geosegnet: point cloud semantic segmentation via geometric encoder–decoder modeling. *The Visual Computer*, 40(8):5107–5121, 2024. 3

[8] Jieneng Chen, Yongyi Lu, Qihang Yu, Xiangde Luo, Ehsan Adeli, Yan Wang, Le Lu, Alan L Yuille, and Yuyin Zhou. Transunet: Transformers make strong encoders for medical image segmentation. *arXiv preprint arXiv:2102.04306*, 2021. 3

[9] Hanyang Chi, Jian Pang, Bingfeng Zhang, and Weifeng Liu. Adaptive bidirectional displacement for semi-supervised medical image segmentation. In *Proceedings of the IEEE/CVF conference on computer vision and pattern recognition*, pages 4070–4080, 2024. 6

[10] Patryk Chlap, Hong Min, Nicholas Vandenberg, Jason Dowling, Lois Holloway, and Annette Haworth. A review of medical image data augmentation techniques for deep learning applications. *Journal of Medical Imaging and Radiation Oncology*, 65(5):545–563, 2021. 1, 3

[11] Terrance DeVries and Graham W Taylor. Improved regularization of convolutional neural networks with cutout. *arXiv preprint arXiv:1708.04552*, 2017. 1, 3, 6

[12] Terrance DeVries and Graham W Taylor. Improved regularization of convolutional neural networks with cutout. *arXiv preprint arXiv:1708.04552*, 2017. 5

[13] Linshuang Diao, Dayong Ren, Sensen Song, and Yurong Qian. Zigzagpointmamba: Spatial-semantic mamba for point cloud understanding. *arXiv preprint arXiv:2505.21381*, 2025. 3

[14] Alexey Dosovitskiy, Lucas Beyer, Alexander Kolesnikov, Dirk Weissenborn, Xiaohua Zhai, Thomas Unterthiner, Mostafa Dehghani, Matthias Minderer, Georg Heigold, Sylvain Gelly, et al. An image is worth 16x16 words: Transformers for image recognition at scale. *arXiv preprint arXiv:2010.11929*, 2020. 2

[15] Yunhe Gao, Mu Zhou, and Dimitris N Metaxas. Utne: a hybrid transformer architecture for medical image segmentation. In *International conference on medical image computing and computer-assisted intervention*, pages 61–71. Springer, 2021. 3

[16] Chengyue Gong, Dilin Wang, Qiang Chen, Zhan Li, Jingdong Yu, Jun Geng, Wei Liu, Yunchao Wang, and Yun Liu. Keepaugment: A simple information-preserving data augmentation approach. In *Proceedings of the IEEE/CVF Conference on Computer Vision and Pattern Recognition (CVPR)*, pages 13484–13493, 2021. 3

[17] Albert Gu and Tri Dao. Mamba: Linear-time sequence modeling with selective state spaces. *arXiv preprint arXiv:2312.00752*, 2023. 3

[18] Yanwen Guo, Yuanqi Li, Dayong Ren, Xiaohong Zhang, Jiawei Li, Liang Pu, Changfeng Ma, Xiaoyu Zhan, Jie Guo, Mingqiang Wei, et al. Lidar-net: A real-scanned 3d point cloud dataset for indoor scenes. In *Proceedings of the IEEE/CVF Conference on Computer Vision and Pattern Recognition*, pages 21989–21999, 2024. 3

[19] Kaiming He, Xinlei Chen, Saining Xie, Yanghao Li, Piotr Dollár, and Ross Girshick. Masked autoencoders are scalable vision learners. In *Proceedings of the IEEE/CVF Conference on Computer Vision and Pattern Recognition (CVPR)*, pages 16000–16009, 2022. 2, 3

[20] Nicholas Heller, Fabian Isensee, Klaus H Maier-Hein, Xiaoshuai Hou, Chunmei Xie, Feng Li, Yang Nan, Gengbo Mu, Zhiyong Lin, Zhangfu Han, et al. The state of the art in kidney and kidney tumor segmentation in contrast-enhanced ct imaging: Results of the kits21 challenge. *Medical Image Analysis*, 84:102685, 2023. 2

[21] Mohammad Hesam Hesamian, Wenjing Jia, Xiangjian He, and Paul Kennedy. Deep learning techniques for medical image segmentation: achievements and challenges. *Journal of digital imaging*, 32(4):582–596, 2019. 1

[22] Huimin Huang, Lanfen Lin, Ruofeng Tong, Hongjie Hu, Qiaowei Zhang, Yutaro Iwamoto, Xianhua Han, Yen-Wei Chen, and Jian Wu. Unet 3+: A full-scale connected unet for medical image segmentation. In *ICASSP 2020-2020 IEEE international conference on acoustics, speech and signal processing (ICASSP)*, pages 1055–1059. Ieee, 2020. 2

[23] Senlong Huang, Yongxin Ge, Dongfang Liu, Mingjian Hong, Junhan Zhao, and Alexander C Loui. Rethinking copy-paste for consistency learning in medical image segmentation. *IEEE Transactions on Image Processing*, 2025. 6

[24] Tao Huang, Xiaohuan Pei, Shan You, Fei Wang, Chen Qian, and Chang Xu. Localmamba: Visual state space model with windowed selective scan. In *European Conference on Computer Vision*, pages 12–22. Springer, 2024. 3

[25] Zeshan Hussain, Francisco Gimenez, Darvin Yi, and Daniel Rubin. Differential data augmentation techniques for medical imaging classification tasks. In *AMIA annual symposium proceedings*, page 979, 2018. 6

[26] Fabian Isensee, Paul F Jaeger, Simon AA Kohl, Jens Petersen, and Klaus H Maier-Hein. nnu-net: a self-configuring method for deep learning-based biomedical image segmentation. *Nature methods*, 18(2):203–211, 2021. 2

[27] Pieter-Jan Kindermans, Sara Hooker, Julius Adebayo, Maximilian Alber, Kristof T Schütt, Tine Dhaene, and Klaus-Robert Müller. The (un) reliability of saliency methods. *Explainable AI: Interpreting, explaining and visualizing deep learning*, pages 267–282, 2019. 3

[28] Wenjie Li, Jia Liu, Wei Hao, Haisong Liu, Dayong Ren, Yanyan Wang, and Lijun Chen. Online deep bingham network for probabilistic orientation estimation. *IET Computer Vision*, 17(6):663–675, 2023. 3

[29] Wenjie Li, Jia Liu, Yanyan Wang, Wei Hao, Dayong Ren, and Lijun Chen. Dl-posenet: A differential lightweight network for pose regression over se (3). In *2024 IEEE International Conference on Robotics and Automation (ICRA)*, pages 16834–16840. IEEE, 2024. 3

[30] Zhan Li, Chunxia Zhang, Yongqin Zhang, Xiaofeng Wang, Xiaolong Ma, Hai Zhang, and Songdi Wu. Can: Context-assisted full attention network for brain tissue segmentation. *Medical Image Analysis*, 85:102710, 2023. 2

[31] Jiarun Liu, Hao Yang, Hong-Yu Zhou, Yan Xi, Lequan Yu, Cheng Li, Yong Liang, Guangming Shi, Yizhou Yu, Shaotong Zhang, et al. Swin-umamba: Mamba-based unet with imagenet-based pretraining. In *International conference on medical image computing and computer-assisted intervention*, pages 615–625. Springer, 2024. 3, 6, 7

[32] Jonathan Long, Evan Shelhamer, and Trevor Darrell. Fully convolutional networks for semantic segmentation. In *Proceedings of the IEEE conference on computer vision and pattern recognition*, pages 3431–3440, 2015. 2

[33] Laurens van der Maaten and Geoffrey Hinton. Visualizing data using t-sne. *Journal of machine learning research*, 9 (Nov):2579–2605, 2008. 8

[34] Daniel S Marcus, Tracy H Wang, Jamie Parker, John G Csernansky, John C Morris, and Randy L Buckner. Open access series of imaging studies (oasis): cross-sectional mri data in young, middle aged, nondemented, and demented older adults. *Journal of cognitive neuroscience*, 19(9):1498–1507, 2007. 5

[35] Adriënne M Mendrik, Koen L Vincken, Hugo J Kuijf, Marcel Breeuwer, Willem H Bouvy, Jeroen De Bresser, Amir Alansary, Marleen De Bruijne, Aaron Carass, Ayman El-Baz, et al. Mrbrains challenge: online evaluation framework for brain image segmentation in 3t mri scans. *Computational intelligence and neuroscience*, 2015(1):813696, 2015. 5

[36] Bjoern H Menze, Andras Jakab, Stefan Bauer, Jayashree Kalpathy-Cramer, Keyvan Farahani, Justin Kirby, Yuliya Burren, Nicole Porz, Johannes Slotboom, Roland Wiest, et al. The multimodal brain tumor image segmentation benchmark (brats). *IEEE transactions on medical imaging*, 34(10):1993–2024, 2014. 2

[37] Dayong Ren, Zhenhong Jia, Jie Yang, and Nikola K Kasabov. A practical grabcut color image segmentation based on bayes classification and simple linear iterative clustering. *IEEE Access*, 5:18480–18487, 2017. 3

[38] Dayong Ren, Zhengyi Wu, Jiawei Li, Piaopiao Yu, Jie Guo, Mingqiang Wei, and Yanwen Guo. Point attention network for point cloud semantic segmentation. *Science China Information Sciences*, 65(9):192104, 2022. 2

[39] Dayong Ren, Shuangyu Yang, Wenjie Li, Jie Guo, and Yanwen Guo. Sae: Estimation for transition matrix in annotation algorithms. *arXiv preprint*, 2022.

[40] Dayong Ren, Zhe Ma, Yuanpei Chen, Weihang Peng, Xiaode Liu, Yuhang Zhang, and Yufei Guo. Spiking pointnet: Spiking neural networks for point clouds. *Advances in Neural Information Processing Systems*, 36, 2024. 2

[41] Olaf Ronneberger, Philipp Fischer, and Thomas Brox. U-net: Convolutional networks for biomedical image segmentation. In *International Conference on Medical Image Computing and Computer-Assisted Intervention (MICCAI)*, pages 234–241. Springer, 2015. 2

[42] Ramprasaath R Selvaraju, Michael Cogswell, Abhishek Das, Ramakrishna Vedantam, Devi Parikh, and Dhruv Batra.

Grad-cam: Visual explanations from deep networks via gradient-based localization. In *Proceedings of the IEEE International Conference on Computer Vision (ICCV)*, pages 618–626, 2017. 3

[43] Connor Shorten and Taghi M Khoshgoftaar. A survey on image data augmentation for deep learning. *Journal of Big Data*, 6(1):1–48, 2019. 1, 3

[44] Karen Simonyan, Andrea Vedaldi, and Andrew Zisserman. Deep inside convolutional networks: Visualising image classification models and saliency maps. *arXiv preprint arXiv:1312.6034*, 2014. 3

[45] Ilyas Siraztdinov, Maksym Kholiavchenko, Ramil Kuleev, and Bulat Ibragimov. Data augmentation for chest pathologies classification. In *2019 IEEE 16th international symposium on biomedical imaging (ISBI 2019)*, pages 1216–1219. IEEE, 2019. 6

[46] Sensen Song, Yurong Qian, Dayong Ren, et al. Zigzag-pointmamba: Spatial-semantic mamba for point cloud understanding. In *The Thirty-ninth Annual Conference on Neural Information Processing Systems*. 1

[47] Sensen Song, Dayong Ren, Zhenhong Jia, and Fei Shi. Adaptive gaussian regularization constrained sparse subspace clustering for image segmentation. In *ICASSP 2024-2024 IEEE International Conference on Acoustics, Speech and Signal Processing (ICASSP)*, pages 4400–4404. IEEE, 2024. 3

[48] D Sun, F Dornaika, and N Barrena. Hsmix: Hard and soft mixing data augmentation for medical image segmentation. *Information Fusion*, 115:102741, 2025. 6

[49] Xu Sun, Huihui Fang, Yehui Yang, Dongwei Zhu, Lei Wang, Junwei Liu, and Yanwu Xu. Robust retinal vessel segmentation from a data augmentation perspective. In *International workshop on ophthalmic medical image analysis*, pages 189–198. Springer, 2021. 6

[50] Yuchao Tang, Yiqin Lu, Bowen Li, Yandong Li, Adway Sankar, Ze Chen, R. F. Wang, and Kevin Chang. Self-supervised pre-training of transformers for digital pathology. *arXiv preprint arXiv:2211.12323*, 2022. 2, 3

[51] David Tellez, Geert Litjens, Péter Bárdi, Wouter Bulten, John-Melle Bokhorst, Francesco Ciompi, and Jeroen Van Der Laak. Quantifying the effects of data augmentation and stain color normalization in convolutional neural networks for computational pathology. *Medical image analysis*, 58:101544, 2019. 6

[52] Jinhong Wang, Jintai Chen, Danny Chen, and Jian Wu. Large window-based mamba unet for medical image segmentation: Beyond convolution and self-attention. *CoRR*, 2024. 3

[53] Zhaohu Xing, Tian Ye, Yijun Yang, Guang Liu, and Lei Zhu. Segmamba: Long-range sequential modeling mamba for 3d medical image segmentation. In *International conference on medical image computing and computer-assisted intervention*, pages 578–588. Springer, 2024. 3

[54] Suorong Yang, Hongchao Yang, Suhan Guo, Furao Shen, and Jian Zhao. Ipf-rda: An information-preserving framework for robust data augmentation. *IEEE Transactions on Pattern Analysis and Machine Intelligence*, 2025. 5

[55] Sangdoo Yun, Dongyoon Han, Seong Joon Oh, Sanghyuk Chun, Junsuk Choe, and Youngjoon Yoo. Cutmix: Regularization strategy to train strong classifiers with localizable features. In *Proceedings of the IEEE/CVF international conference on computer vision*, pages 6023–6032, 2019. 6

[56] Feifei Zhang, Fei Shi, Dayong Ren, Zhenhong Jia, and Jianyi Wang. Dual-mambanet: A lightweight dual-branch brain image segmentation network based on local attention and mamba. In *International Conference on Pattern Recognition*, pages 92–107. Springer, 2024. 3

[57] Feifei Zhang, Zhenhong Jia, Sensen Song, Fei Shi, and Dayong Ren. Rethinking convergence in deep learning: The predictive-corrective paradigm for anatomy-informed brain mri segmentation. *arXiv preprint arXiv:2510.15439*, 2025. 1

[58] Feifei Zhang, Fei Shi, Dayong Ren, and Yue Li. A fuzzy c-means clustering algorithm for real medical image segmentation. In *ICASSP 2025-2025 IEEE International Conference on Acoustics, Speech and Signal Processing (ICASSP)*, pages 1–5. IEEE, 2025. 1

[59] Hongyi Zhang, Moustapha Cisse, Yann N Dauphin, and David Lopez-Paz. mixup: Beyond empirical risk minimization. In *International Conference on Learning Representations (ICLR)*, 2018. 1, 6

[60] Zhun Zhong, Liang Zheng, Guoliang Kang, Shaozi Li, and Yi Yang. Random erasing data augmentation. In *Proceedings of the AAAI Conference on Artificial Intelligence (AAAI)*, 34(07):13001–13008, 2020. 1, 3, 6

[61] Nan Zhou, Mingming Xu, Biaoqun Shen, Ke Hou, Shanwei Liu, Hui Sheng, Yanfen Liu, and Jianhua Wan. Vit-unet: A vision transformer based unet model for coastal wetland classification based on high spatial resolution imagery. *IEEE Journal of Selected Topics in Applied Earth Observations and Remote Sensing*, 2024. 3

[62] Zongwei Zhou, Md Mahfuzur Rahman Siddiquee, Nima Tajbakhsh, and Jianming Liang. Unet++: A nested u-net architecture for medical image segmentation. In *International workshop on deep learning in medical image analysis*, pages 3–11. Springer, 2018. 2

[63] Lianghui Zhu, Bencheng Liao, Qian Zhang, Xinlong Wang, Wenyu Liu, and Xinggang Wang. Vision mamba: Efficient visual representation learning with bidirectional state space model. *arXiv preprint arXiv:2401.09417*, 2024. 2

Keep the Core: Adversarial Priors for Significance-Preserving Brain MRI Segmentation

Supplementary Material

6. Extended Experimental Results

In this appendix, we provide the complete and unabridged quantitative results that support the consolidated findings presented in the main paper. The following tables provide an exhaustive, side-by-side comparison of all 12 baseline augmentation methods against their "Keep the Core" (KC) counterparts. The analysis is structured by backbone architecture to demonstrate the universal applicability and scaling advantages of our framework.

6.1. Deeper Analysis: Validating Our Core Motivation

Before breaking down results by backbone, we validate our central hypothesis: standard augmentations can be destructive, and "Keep the Core" (KC) mitigates this. We predict two main effects: (1) KC will "rescue" performance from destructive, information-erasing augmentations, and (2) KC will stabilize high-capacity SOTA models on complex datasets.

Evidence for the "Recovery Effect" We can see this clearly on the SwinUNet backbone with the OASIS-1 dataset (Tab. 7).

- **Gentle Augmentations:** Methods like 'Gaussian Noise' ($0.9129 \rightarrow 0.9131$) or 'Cutout' ($0.9141 \rightarrow 0.9144$) show minimal gains. The dataset is simple and the augmentations are not overly harmful, so KC has little damage to prevent.
- **Destructive Augmentations:** 'Random Erasing' is a clear outlier. Its application causes a significant performance drop (from 0.9145 baseline to 0.9085 GM Dice). This is a perfect example of an "unaware" augmentation corrupting key information. Tellingly, our '**KC-Random Erasing**' (**0.9124**) almost entirely recovers this loss, proving that our method is successfully identifying and protecting the salient anatomical features that the baseline method was destroying.

Evidence for the "SOTA Stabilization Effect" This effect is most evident on the challenging **MRBrainS13 dataset** with the **SwinUMamba backbone** (Tab. 9). Here, the model is highly complex and the data is difficult.

- The baseline model is *extremely sensitive* to augmentation noise. Even "gentle" augmentations like 'Gaussian Noise' (0.6961) and 'Gaussian Blur' (0.7014) result in

GM Dice scores far below the non-augmented baseline (0.7007). The model is clearly confused.

- Our KC framework provides a *massive, universal boost*. 'KC-Gaussian Noise' jumps to 0.7220, and 'KC-Gaussian Blur' jumps to 0.7217.
- This pattern holds for *every single augmentation*. The KC variants are not just better; they are in a different performance class entirely. This proves our hypothesis: for SOTA models on complex tasks, a significance-preserving framework is not just a "tweak" but a *necessity* to stabilize training and prevent the model from learning from noise.

With this validated motivation, we now analyze the per-backbone results in detail.

6.2. Analysis for UNet Backbone (Tables 5 & 6)

As shown in Tab. 5 and Tab. 6, the UNet backbone, representing a classic CNN architecture, serves as a fundamental baseline. On the relatively simple **OASIS-1 dataset**, our KC framework provides consistent and clear improvements. For instance, KC-Cutout improves the baseline Cutout across all primary metrics, notably boosting WM Dice from 0.9212 to 0.9293 and reducing HD95 from 2.1083mm to 1.9644mm.

The benefits are substantially more pronounced on the more challenging **MRBrainS13 dataset**. Here, standard augmentations sometimes offer marginal gains or even degrade performance, whereas the KC variants provide robust enhancements. A clear example is KC-MRS, which improves Dice (GM) from 0.7172 to 0.7210 and dramatically cuts the ASD (WM) from 1.9747mm down to 1.5167mm. Similarly, KC-ABD achieves a large reduction in HD95 (WM) from 4.3564mm to 3.4333mm. The supplementary metrics in Tab. 6 (Accuracy, Precision, Sensitivity, Specificity) corroborate these findings, showing holistic performance gains.

6.3. Analysis for SwinUNet Backbone (Tables 7 & 8)

Upon transitioning to the Transformer-based SwinUNet backbone (Tab. 7 and Tab. 8), we observe that the baseline performance is stronger, yet our KC framework continues to deliver significant advantages.

On **OASIS-1**, the improvements are stable. As discussed in our motivational analysis, the most significant gain comes from **KC-Random Erasing**, which recovers the performance drop seen in its baseline counterpart, bringing

the Dice (GM) from 0.9085 back up to 0.9124.

Once again, the **MRBrainS13 dataset** highlights the framework’s true strength. The KC enhancements are dramatic, especially for mixing-based and erasing-based methods. KC-HSMix, for example, is a star performer: it elevates Dice (GM) from 0.6917 to 0.7063 and slashes the HD95 (GM) from 3.4378mm to an impressive 1.6678mm. Likewise, KC-Cutmix boosts Dice (CSF) from 0.6641 to 0.6744 and reduces ASD (WM) from 2.3117mm to 1.9485mm. This demonstrates our method’s critical ability to stabilize and enhance advanced augmentations on complex architectures.

6.4. Analysis for SwinUMamba Backbone (Tables 9 & 10)

Tab. 9 and Tab. 10 detail the results on the state-of-the-art (SOTA) SwinUMamba backbone. This analysis is crucial, as it tests our framework’s ability to improve an already highly optimized model.

On **OASIS-1**, where performance is approaching saturation (baseline Dice scores are already $\sim 0.92\text{-}0.93$), our KC methods provide consistent, incremental gains that “polish” the SOTA results. For example, KC-MRS raises the WM Dice from 0.9349 to 0.9373 and KC-Cutout raises the CSF Dice from 0.9229 to 0.9262.

The most compelling evidence is found on the **MR-BrainS13 dataset**. As predicted by our “SOTA Stabilization Effect,” the baseline SwinUMamba, while strong, is significantly elevated by our framework across the board. The improvements are not incremental; they are substantial.

- **KC-ABD** boosts the WM Dice from 0.6976 to 0.7381. More strikingly, it reduces the corresponding ASD (Average Surface Distance) from 3.0102mm to a mere **0.4790mm**—a 6.3x reduction.
- **KC-MRS** achieves the highest CSF Dice (0.7024 vs. 0.6864) and GM Dice (0.7207 vs. 0.7068) among its peers.
- **KC-Bias Field** shows a massive jump in WM Dice (0.7233 to 0.7525) and a large drop in WM HD95 (5.2166mm to 3.7876mm).

This focus on the distance metrics (ASD/HD95) is critical. A good Dice score means “most” of the segmentation is correct, but a poor HD95/ASD score means the model has severe “outlier” errors at the boundaries. Our method’s dramatic improvements here are the strongest possible evidence for our motivation: by protecting the “core” anatomy, we are specifically preserving the complex, difficult-to-segment boundaries that standard augmentations corrupt. These results conclusively demonstrate that our significance-preserving approach is a vital component for unlocking the full potential of SOTA architectures on complex, clinically-relevant data.

7. Qualitative Evaluation

Fig. 7 and Fig. 8 provide qualitative comparisons on the OASIS-1 and MRBrainS13 datasets, respectively. It is visually evident that the baseline predictions (c) and standard augmentations (e.g., (d), (g), (i)) frequently suffer from noisy artifacts, blurred boundaries, and mis-segmentation of intricate anatomical structures. In stark contrast, our “Ours+” enhanced methods (e.g., (e), (h), (k)) consistently produce segmentation maps that are visibly cleaner, more spatially coherent, and demonstrate significantly sharper adherence to the Ground Truth (b). This superior fidelity is particularly noticeable in the complex sulcal patterns and holds true across all three backbones (rows), confirming that our framework yields more robust and anatomically plausible results.

8. Class Activation Map (CAM) Analysis

Since class activation maps (CAM) visualization can provide visual explanations for understanding model performance, we incorporate CAM visualization as a tool to analyze the discriminative regions used by our models. We compare the performance of baseline augmentation strategies against their “Ours+” enhanced counterparts. Fig. 9 and Fig. 10 illustrate the CAMs generated from models trained on the OASIS-1 and MRBrainS13 datasets. It is visually evident that the baseline models’ (e.g., rows 1, 3, 5) regions of interest are often highly diffuse and noisy. They cover irrelevant textures or artifacts and seem distracted from the core anatomical structures, indicating a potential overfitting problem and poor generalization. In contrast, after utilizing our framework, the “Ours+” models (rows 2, 4, 6) are more inclined to locate and highlight the most relevant parts of the target anatomy (e.g., Gray Matter or White Matter). These methods’ regions of interest are significantly more focused, structurally coherent, and precisely localized, while ignoring much of the spurious background information. This indicates a better generalization ability. To summarize, these visualizations underscore how our framework surpasses the efficacy of the original augmentation methodologies, forcing the model to learn true, generalizable anatomical representations, which in turn explains the more robust and accurate segmentation performance.

9. Computational Cost Analysis.

We analyze the computational overhead in Fig. 11. A key advantage of our Keep the Core framework is that it introduces no additional latency during the online stage, which is the most critical part of practical usage. As shown in Fig. 11(b), the online inference time of our method remains identical to the baselines on both MRBrainS13 and OASIS-1. The radar chart in Fig. 11(a) further summarizes

computation-related factors—including model size, FLOPs, training and inference times, and throughput—showing that our modifications do not impose any extra online computation burden. Although our approach requires an offline preprocessing step to generate importance maps, this cost is paid once per dataset and is fully amortized across experiments, leaving the practical training and inference budgets unchanged.

Table 5. Quantitative comparison of different methods under the same backbone(UNet) on the OASIS-1 and MRBrainS13 test sets. In the table, the best-performing metrics of our method and its corresponding baseline are highlighted in bold.

Model	Dice \uparrow			HD95(mm) \downarrow			ASD(mm) \downarrow			IOU \uparrow		
	CSF	GM	WM	CSF	GM	WM	CSF	GM	WM	CSF	GM	WM
OASIS-1 dataset												
UNet	0.9062	0.9134	0.9181	1.1267	1.2138	2.0824	0.2581	0.3611	0.6198	0.8442	0.8599	0.8688
Gaussian noise	0.9038	0.9141	0.9227	1.1452	1.1815	1.9931	0.2588	0.3466	0.5883	0.8403	0.8613	0.8748
Keep the core-Gaussian noise	0.9077	0.9164	0.9228	1.1019	1.1495	2.0568	0.2571	0.3462	0.5788	0.8463	0.8643	0.8749
Gaussian blur	0.9056	0.9109	0.9195	1.1286	1.2059	2.0272	0.2630	0.3684	0.6007	0.8429	0.8558	0.8693
Keep the core-Gaussian blur	0.9087	0.9139	0.9211	1.1024	1.1795	2.0216	0.2574	0.3548	0.6004	0.8478	0.8600	0.8717
Gamma	0.8983	0.9041	0.9150	1.2218	1.2744	2.5047	0.2668	0.3857	0.7989	0.8316	0.8474	0.8630
Keep the core-Gamma	0.9041	0.9064	0.9171	1.1828	1.2732	2.3185	0.2664	0.3851	0.7621	0.8416	0.8507	0.8659
Brightness contrast	0.9078	0.9138	0.9193	1.1229	1.1742	2.1301	0.2623	0.3578	0.6197	0.8486	0.8601	0.8704
Keep the core-Brightness contrast	0.9083	0.9146	0.9193	1.1220	1.1674	2.1252	0.2582	0.3535	0.6009	0.8463	0.8604	0.8714
Bias files	0.9066	0.9138	0.9191	1.1410	1.1991	1.9811	0.2568	0.3536	0.5590	0.8446	0.8605	0.8705
Keep the core-Bias files	0.9068	0.9140	0.9212	1.1408	1.1869	2.0088	0.2514	0.3530	0.5507	0.8448	0.8607	0.8724
Random Erasing	0.9049	0.9134	0.9181	1.1483	1.2358	2.1140	0.2651	0.3631	0.6412	0.8419	0.8588	0.8719
Keep the core-RandomErasing	0.9095	0.9089	0.9162	1.1346	1.2898	2.1017	0.2620	0.3606	0.6149	0.8428	0.8596	0.9731
Cutout	0.9081	0.9132	0.9212	1.1342	1.2213	2.1083	0.2667	0.3675	0.6290	0.8472	0.8594	0.8719
Keep the core-Cutout	0.9099	0.9135	0.9293	1.1006	1.1940	1.9644	0.2624	0.3618	0.5620	0.8498	0.8596	0.8797
Mixup	0.9037	0.9091	0.9174	1.1937	1.2792	2.1584	0.2753	0.3794	0.6745	0.8408	0.8534	0.8661
Keep the core-Mixup	0.9039	0.9098	0.9188	1.1524	1.2728	2.1581	0.2674	0.3772	0.6723	0.8485	0.8540	0.8561
Cutmix	0.9068	0.9164	0.9240	1.1057	1.1653	1.9241	0.2652	0.3454	0.5723	0.8442	0.8643	0.8766
Keep the core-Cutmix	0.9074	0.9170	0.9241	1.1055	1.1622	1.8766	0.2612	0.3452	0.5224	0.8456	0.8651	0.8767
HSMix	0.9030	0.9121	0.9193	1.1761	1.2485	2.0038	0.2873	0.3572	0.5753	0.8394	0.8583	0.8695
Keep the core-HSMix	0.9118	0.9126	0.9194	1.1717	1.2382	2.0966	0.2798	0.3531	0.6351	0.8395	0.8584	0.8696
MRS	0.9036	0.9156	0.9210	1.1537	1.1940	1.9734	0.2721	0.3501	0.5304	0.8394	0.8630	0.8731
Keep the core-MRS	0.9085	0.9166	0.9213	1.1448	1.1913	2.0266	0.2720	0.3500	0.5425	0.8395	0.8671	0.8706
ABD	0.9084	0.9117	0.9168	1.1232	1.1973	2.0758	0.2555	0.3679	0.6462	0.8471	0.8554	0.8648
Keep the core-ABD	0.9087	0.9134	0.9211	1.1217	1.1944	2.0456	0.2507	0.3564	0.6034	0.8779	0.8594	0.8718
MRBrainS13 dataset												
UNet	0.6947	0.7104	0.7309	1.9670	2.5323	4.7501	0.4383	0.6621	2.0734	0.6115	0.6367	0.6637
Gaussian noise	0.7030	0.7228	0.7482	1.7150	1.7318	4.2805	0.4114	0.4081	1.5736	0.6233	0.6536	0.6807
Keep the core-Gaussian noise + UNet	0.7040	0.7238	0.7493	1.7144	1.6600	3.7758	0.4040	0.3960	1.1133	0.6235	0.6585	0.6891
Gaussian blur	0.7043	0.7234	0.7411	1.6470	1.5681	3.9442	0.4148	0.3935	1.3125	0.6250	0.6542	0.6740
Keep the core-Gaussian blur	0.7063	0.7255	0.7435	1.6356	1.5476	3.8752	0.4173	0.4006	1.1354	0.6323	0.6586	0.6756
Gamma	0.7034	0.7213	0.7409	1.6832	1.5088	3.6378	0.4286	0.4021	1.3495	0.6237	0.6508	0.6734
Keep the core-Gamma	0.7039	0.7198	0.7414	1.6382	1.6529	3.6230	0.4188	0.4252	1.2716	0.6244	0.6593	0.6737
Brightness contrast	0.7028	0.7210	0.7445	1.7027	1.6027	3.7314	0.4118	0.4021	1.5862	0.6228	0.6507	0.6761
Keep the core-Brightness contrast	0.7075	0.7260	0.7414	1.6739	1.5791	3.0973	0.4102	0.3646	1.0075	0.6211	0.6537	0.6786
Bias files	0.7015	0.7167	0.7440	1.7650	2.2214	2.8878	0.4323	0.5480	0.8531	0.6210	0.6447	0.6759
Keep the core-Bias files	0.7022	0.7199	0.7421	1.7358	2.0646	3.3793	0.4231	0.5475	1.0747	0.6218	0.6490	0.6726
Random Erasing	0.6932	0.7124	0.7451	1.9145	2.4821	4.0623	0.4276	0.6126	1.5925	0.6125	0.6431	0.6742
Keep the core-RandomErasing	0.6884	0.7131	0.7508	2.0715	1.9541	3.4860	0.4468	0.4451	0.8917	0.6045	0.6388	0.6781
Cutout	0.7020	0.7202	0.7465	1.7482	1.7951	4.8972	0.4057	0.5518	1.3804	0.6219	0.6495	0.6774
Keep the core-Cutout	0.7020	0.7291	0.7501	1.7067	1.6769	4.2185	0.4108	0.4156	1.0678	0.6215	0.6494	0.6808
Mixup	0.6987	0.7188	0.7370	1.8542	1.6421	3.7362	0.4505	0.4085	1.3004	0.6163	0.6471	0.6659
Keep the core-Mixup	0.7003	0.7208	0.7411	1.8090	1.6385	3.5453	0.4169	0.4080	0.7595	0.6186	0.6506	0.6710
Cutmix	0.6973	0.7177	0.7385	1.8972	1.6684	3.1470	0.4220	0.4150	1.2437	0.6145	0.6456	0.6700
Keep the core-Cutmix	0.6987	0.7190	0.7489	1.8443	1.6369	3.3379	0.4373	0.4118	1.1686	0.6164	0.6470	0.6774
HSMix	0.6943	0.7180	0.7350	2.0023	1.7585	2.9688	0.4504	0.4177	0.6587	0.6097	0.6456	0.6633
Keep the core-HSMix	0.6956	0.7182	0.7390	1.9695	1.7424	2.4250	0.4495	0.4151	0.6419	0.6116	0.6459	0.6680
MRS	0.7002	0.7172	0.7399	1.8441	2.0810	4.5415	0.4127	0.4927	1.9747	0.6187	0.6444	0.6687
Keep the core-MRS	0.7023	0.7210	0.7449	1.7543	1.5547	3.6870	0.4113	0.3959	1.5167	0.6221	0.6502	0.6765
ABD	0.7034	0.7189	0.7500	1.6590	2.1227	4.3564	0.4150	0.5158	1.6365	0.6236	0.6481	0.6813
Keep the core-ABD	0.7040	0.7216	0.7522	1.6176	1.5557	3.4333	0.4140	0.4003	1.2089	0.6243	0.6513	0.6831

Table 6. Quantitative comparison of different methods under the same backbone(UNet) on the OASIS-1 and MRBrainS13 test sets. In the table, the best-performing metrics of our method and its corresponding baseline are highlighted in bold.

Model	Acc↑			Pre↑			Sen↑			Spe↑		
	CSF	GM	WM									
OASIS-1 dataset												
UNet	0.9732	0.9655	0.9844	0.9332	0.9155	0.9174	0.8838	0.9140	0.9331	0.9791	0.9711	0.9866
Gaussian noise	0.9729	0.9655	0.9851	0.9336	0.9154	0.9245	0.8791	0.9158	0.9326	0.9791	0.9707	0.9876
Keep the core-Gaussian noise	0.9734	0.9659	0.9854	0.9382	0.9184	0.9314	0.9003	0.9165	0.9345	0.9792	0.9713	0.9881
Gaussian blur	0.9730	0.9643	0.9840	0.9369	0.9134	0.9104	0.8795	0.9110	0.9422	0.9795	0.9702	0.9857
Keep the core-Gaussian blur	0.9737	0.9658	0.9847	0.9379	0.9174	0.9135	0.8874	0.9127	0.9424	0.9796	0.9718	0.9867
Gamma	0.9721	0.9641	0.9845	0.9422	0.9101	0.8934	0.8622	0.9026	0.9526	0.9787	0.9706	0.9860
Keep the core-Gamma	0.9724	0.9642	0.9849	0.9424	0.9160	0.8959	0.8821	0.9029	0.9535	0.9789	0.9718	0.9868
Brightness contrast	0.9733	0.9656	0.9838	0.9302	0.9158	0.9169	0.8897	0.9140	0.9342	0.9790	0.9717	0.9857
Keep the core-Brightness contrast	0.9737	0.9657	0.9836	0.9437	0.9173	0.9090	0.8899	0.9146	0.9541	0.9798	0.9718	0.9859
Bias fields	0.9733	0.9655	0.9845	0.9346	0.9142	0.9229	0.8832	0.9162	0.9295	0.9794	0.9711	0.9866
Keep the core-Bias fields	0.9734	0.9656	0.9848	0.9348	0.9144	0.9229	0.8834	0.9176	0.9330	0.9795	0.9717	0.9876
Random Erasing	0.9732	0.9653	0.9846	0.9312	0.9243	0.9075	0.8831	0.9053	0.9484	0.9789	0.9728	0.9858
Keep the core-RandomErasing	0.9735	0.9630	0.9856	0.9425	0.8862	0.8969	0.8838	0.9058	0.9497	0.9797	0.9735	0.9864
Cutout	0.9736	0.9654	0.9846	0.9280	0.9217	0.9103	0.8920	0.9077	0.9447	0.9789	0.9724	0.9862
Keep the core-Cutout	0.9738	0.9658	0.9849	0.9303	0.9295	0.9156	0.8922	0.9095	0.9465	0.9792	0.9742	0.9867
Mixup	0.9722	0.9639	0.9837	0.9351	0.9218	0.9008	0.8783	0.9008	0.9490	0.9785	0.9725	0.9840
Keep the core-Mixup	0.9725	0.9637	0.9838	0.9380	0.9245	0.8939	0.8757	0.9010	0.9577	0.9792	0.9734	0.9846
Cutmix	0.9736	0.9664	0.9854	0.9303	0.9150	0.9270	0.8868	0.9201	0.9335	0.9792	0.9708	0.9891
Keep the core-Cutmix	0.9738	0.9665	0.9858	0.9317	0.9152	0.9394	0.8898	0.9254	0.9350	0.9898	0.9728	0.9900
HSMix	0.9733	0.9653	0.9847	0.9259	0.9181	0.9257	0.8864	0.9108	0.9281	0.9788	0.9717	0.9876
Keep the core-HSMix	0.9734	0.9653	0.9848	0.9315	0.9184	0.9258	0.8880	0.9136	0.9293	0.9793	0.9718	0.9878
MRS	0.9734	0.9662	0.9854	0.9324	0.9142	0.9323	0.8798	0.9195	0.9238	0.9793	0.9711	0.9886
Keep the core-MRS	0.9738	0.9663	0.9846	0.9376	0.9149	0.9381	0.8799	0.9199	0.9343	0.9797	0.9713	0.9886
ABD	0.9737	0.9646	0.9834	0.9342	0.9236	0.9039	0.8867	0.9024	0.9447	0.9794	0.9730	0.9842
Keep the core-ABD	0.9739	0.9657	0.9839	0.9376	0.9239	0.9149	0.8936	0.9061	0.9495	0.9795	0.9735	0.9854
MRBrainS13 dataset												
UNet	0.7967	0.7938	0.8966	0.7086	0.7056	0.717	0.6852	0.7180	0.7748	0.8051	0.8016	0.8990
Gaussian noise	0.7975	0.7957	0.9080	0.7097	0.7194	0.7706	0.6979	0.7270	0.7535	0.8050	0.8027	0.9115
Keep the core-Gaussian noise	0.7976	0.7959	0.9170	0.7105	0.7277	0.7890	0.6987	0.7349	0.7584	0.8051	0.8027	0.8905
Gaussian blur	0.7976	0.7956	0.8870	0.7085	0.7189	0.7676	0.7017	0.7290	0.7466	0.8048	0.8026	0.8905
OKeep the core-Gaussian blur	0.7976	0.7957	0.8871	0.7143	0.7773	0.7688	0.7029	0.7246	0.7587	0.8054	0.8027	0.8983
Gamma	0.7973	0.7954	0.8871	0.6972	0.7249	0.7407	0.7122	0.7185	0.7503	0.8037	0.8033	0.8903
Keep the core-Gamma	0.7975	0.7954	0.8766	0.7057	0.7360	0.7419	0.7240	0.7196	0.7534	0.8046	0.8081	0.9096
Brightness contrast	0.7975	0.7954	0.8975	0.7083	0.7186	0.7464	0.6991	0.7247	0.7575	0.8049	0.8027	0.9005
Keep the core-Brightness contrast	0.7976	0.7958	0.9178	0.7087	0.7278	0.7477	0.7065	0.7256	0.7649	0.8058	0.8042	0.9203
Bias fields	0.7972	0.7950	0.8869	0.7001	0.7253	0.7430	0.7053	0.7092	0.7443	0.8041	0.8037	0.8895
Keep the core-Bias fields	0.7973	0.7953	0.9078	0.7057	0.7201	0.7631	0.7068	0.7208	0.7460	0.8046	0.8031	0.9114
Random Erasing	0.7970	0.7948	0.8969	0.7118	0.7089	0.7480	0.6858	0.7185	0.7706	0.8051	0.8023	0.8999
Keep the core-RandomErasing	0.7963	0.7953	0.8999	0.7079	0.7096	0.7485	0.6789	0.7231	0.7839	0.8049	0.8045	0.9012
Cutout	0.7975	0.7951	0.8972	0.7120	0.7196	0.7545	0.6939	0.7223	0.7565	0.8053	0.8028	0.9002
Keep the core-Cutout	0.7975	0.7953	0.9077	0.7124	0.7168	0.7691	0.6993	0.7224	0.7663	0.8053	0.8129	0.9109
Mixup	0.7964	0.7949	0.8762	0.6901	0.7202	0.7521	0.7105	0.7187	0.7382	0.8031	0.8028	0.8800
Keep the core-Mixup	0.7970	0.7953	0.8763	0.7043	0.7237	0.7600	0.7115	0.7292	0.7446	0.8045	0.8029	0.8999
Cutmix	0.7969	0.7947	0.8555	0.7117	0.7141	0.7322	0.6857	0.7224	0.7574	0.8053	0.8023	0.8583
Keep the core-Cutmix	0.7969	0.7948	0.8761	0.7093	0.7162	0.7464	0.6906	0.7229	0.7631	0.8061	0.8025	0.8790
HSMix	0.7961	0.7945	0.8551	0.6967	0.7129	0.7456	0.6957	0.7250	0.7447	0.8039	0.8020	0.8536
Keep the core-HSMix	0.7962	0.7947	0.8650	0.6979	0.7263	0.7464	0.7000	0.7268	0.7491	0.8135	0.8024	0.8587
MRS	0.7972	0.7946	0.8966	0.7115	0.7160	0.7426	0.6912	0.7201	0.7681	0.8053	0.8026	0.8990
Keep the core-MRS	0.7973	0.7954	0.8974	0.7154	0.7240	0.7462	0.7012	0.7193	0.7698	0.8055	0.8034	0.9004
ABD	0.7975	0.7952	0.9077	0.7062	0.7214	0.7420	0.7021	0.7174	0.7667	0.8045	0.8034	0.9106
OKeep the core-ABD	0.7979	0.7953	0.9095	0.7090	0.7267	0.7588	0.7067	0.7273	0.7686	0.8049	0.8082	0.9102

Table 7. Quantitative comparison of different methods under the same backbone(SwinUNet) on the OASIS-1 and MRBrainS13 test sets. In the table, the best-performing metrics of our method and its corresponding baseline are highlighted in bold.

Model	Dice \uparrow			HD95(mm) \downarrow			ASD(mm) \downarrow			IOU \uparrow		
	CSF	GM	WM	CSF	GM	WM	CSF	GM	WM	CSF	GM	WM
OASIS-1 dataset												
SwinUNet	0.9051	0.9145	0.9226	1.1233	1.1778	1.7979	0.2966	0.3501	0.5340	0.8425	0.8619	0.8743
Gaussian noise	0.9041	0.9129	0.9199	1.1360	1.2119	1.8900	0.3062	0.3605	0.5480	0.8403	0.8591	0.8703
Keep the core-Gaussian noise	0.9043	0.9131	0.9221	1.1357	1.2108	1.7789	0.3061	0.3601	0.5478	0.8406	0.8596	0.8713
Gaussian blur	0.9074	0.9153	0.9216	1.1320	1.1877	1.7252	0.3029	0.3499	0.4994	0.8464	0.8629	0.8732
Keep the core-Gaussian blur	0.9077	0.9154	0.9218	1.1297	1.1866	1.7139	0.3026	0.3483	0.4991	0.8468	0.8630	0.8735
Gamma	0.8990	0.9106	0.9167	1.1511	1.2452	1.9767	0.3140	0.3787	0.5533	0.8318	0.8547	0.8652
Keep the core-Gamma	0.9001	0.9112	0.9169	1.1503	1.2445	1.9763	0.3408	0.3781	0.5531	0.8316	0.8546	0.8653
Brightness contrast	0.9051	0.9134	0.9197	1.1264	1.2000	1.8744	0.2982	0.3577	0.5460	0.8423	0.8600	0.8704
Keep the core-Brightness contrast	0.9053	0.9135	0.9199	1.1261	1.1997	1.8731	0.2981	0.3572	0.5457	0.8423	0.8601	0.8707
Bias fields	0.9086	0.9166	0.9202	1.0957	1.1650	1.8014	0.2770	0.3356	0.4693	0.8478	0.8649	0.8719
Keep the core-Bias fields	0.9181	0.9168	0.9203	1.0959	1.1584	1.7925	0.2768	0.3355	0.4690	0.8479	0.8653	0.8923
Random Erasing	0.8989	0.9085	0.9150	1.1831	1.2965	2.1528	0.3351	0.3998	0.6200	0.8316	0.8516	0.8622
Keep the core-RandomErasing	0.9033	0.9124	0.9193	1.1349	1.2193	1.9367	0.3033	0.3756	0.5915	0.8388	0.8580	0.8692
Cutout	0.9051	0.9141	0.9206	1.1374	1.2082	1.8492	0.3080	0.3652	0.5526	0.8418	0.8604	0.8713
Keep the core-Cutout	0.9053	0.9144	0.9216	1.1371	1.2079	1.8049	0.3077	0.3649	0.5525	0.8417	0.8607	0.8717
Mixup	0.8999	0.9118	0.9200	1.2108	1.2968	2.2539	0.3116	0.3835	0.6733	0.8338	0.8581	0.8712
Keep the core-Mixup	0.9002	0.9121	0.9203	1.1905	1.2953	2.2520	0.3106	0.3827	0.6731	0.8339	0.8487	0.8714
Cutmix	0.9097	0.9182	0.9258	1.1309	1.1685	1.6913	0.2755	0.3299	0.4516	0.8513	0.8688	0.8796
Keep the core-Cutmix	0.9113	0.9187	0.9230	1.1297	1.1683	1.6910	0.2748	0.3188	0.4512	0.8517	0.8691	0.8798
HSMix	0.9067	0.9109	0.9174	1.1576	1.2906	2.0383	0.3118	0.3555	0.5315	0.8454	0.8569	0.8665
Keep the core-HSMix	0.9123	0.9112	0.9175	1.1471	1.1998	2.0381	0.3101	0.3541	0.5315	0.8489	0.8571	0.8666
MRS	0.9087	0.9183	0.9240	1.0909	1.1563	1.7596	0.2787	0.3285	0.4893	0.8493	0.8685	0.8772
Keep the core-MRS	0.9095	0.9201	0.9423	1.0902	1.1561	1.7591	0.2784	0.3284	0.4889	0.8497	0.8692	0.8774
ABD	0.9044	0.9146	0.9221	1.1648	1.1972	1.8053	0.2972	0.3455	0.5326	0.8424	0.8628	0.8739
Keep the core-ABD	0.9061	0.9153	0.9232	1.1566	1.1871	1.8049	0.2921	0.3377	0.5318	0.8426	0.8629	0.8741
MRBrainS13 dataset												
SwinUNet	0.6659	0.6936	0.7098	2.3639	3.4329	5.2567	0.5767	0.9310	2.1417	0.5710	0.6151	0.6341
Gaussian noise	0.6606	0.6900	0.6883	2.4726	3.4559	6.2215	0.6631	0.9512	2.4200	0.5634	0.6073	0.6114
Keep the core-Gaussian noise	0.6686	0.6957	0.7067	2.2728	2.8851	5.3106	0.5760	0.7570	2.3405	0.5734	0.6135	0.6302
Gaussian blur	0.6639	0.6928	0.7001	2.3789	3.0653	7.2002	0.6090	0.7770	3.4630	0.5671	0.6100	0.6215
Keep the core-Gaussian blur	0.6639	0.6936	0.7043	2.3546	3.0597	7.0595	0.6025	0.7765	2.7829	0.5669	0.6101	0.6237
Gamma	0.6666	0.6959	0.7099	2.3750	2.9461	5.4661	0.5879	0.7367	2.2741	0.5711	0.6167	0.6358
Keep the core-Gamma	0.6670	0.6976	0.6986	2.2544	2.8887	6.1727	0.5698	0.7216	2.5124	0.5717	0.6168	0.6346
Brightness contrast	0.6541	0.6857	0.7015	3.6086	4.4464	6.3448	1.0888	1.8524	2.2918	0.5581	0.6037	0.6186
Keep the core-Brightness contrast	0.6678	0.7014	0.7040	2.2210	3.0987	6.1291	0.5647	0.9430	2.2154	0.5724	0.6215	0.6238
Bias fields	0.6576	0.6917	0.6928	2.7573	3.3390	5.9294	0.6846	0.8422	2.2025	0.5592	0.6058	0.6096
Keep the core-Bias fields	0.6581	0.6946	0.6996	2.7116	3.3360	6.6131	0.6159	0.8401	2.2645	0.5620	0.6064	0.6094
Random Erasing	0.6379	0.6764	0.6891	3.1546	3.8135	7.0110	0.7391	1.1137	2.6193	0.5376	0.5906	0.6110
Keep the core-RandomErasing	0.6522	0.6900	0.6968	2.7737	3.6032	6.3603	0.6761	1.1103	2.6155	0.5521	0.6048	0.6177
Cutout	0.6698	0.6996	0.6887	2.2273	2.8997	4.9019	0.5709	0.7580	1.9812	0.5754	0.6186	0.6146
Keep the core-Cutout	0.6704	0.6702	0.6911	2.2637	2.5207	4.9009	0.5703	0.6614	1.9506	0.5777	0.6195	0.6148
Mixup	0.6539	0.6935	0.6755	2.7834	3.2271	4.8766	0.6290	0.9504	1.2116	0.5551	0.6093	0.6047
Keep the core-Mixup	0.6567	0.6970	0.6879	2.6986	2.9108	4.7235	0.6145	0.7605	1.1984	0.5584	0.6135	0.6143
Cutmix	0.6641	0.6963	0.6880	2.6508	3.3040	5.8713	0.5965	0.9968	2.3117	0.5674	0.6141	0.6163
Keep the core-Cutmix	0.6744	0.7052	0.7165	2.1924	2.9208	4.8745	0.5446	0.7911	1.9485	0.5815	0.6264	0.6405
HSMix	0.6640	0.6917	0.6903	2.5743	3.4378	4.9869	0.6158	1.0094	1.9139	0.5671	0.6087	0.6171
Keep the core-HSMix	0.6787	0.7063	0.7095	2.1474	1.6678	4.1721	0.5202	0.7576	1.1763	0.5870	0.6282	0.6350
MRS	0.6679	0.6969	0.7041	2.3042	3.2667	5.9343	0.5741	1.0011	2.5644	0.5721	0.6157	0.6274
Keep the core-MRS	0.6683	0.7024	0.7055	2.3026	2.7319	4.9050	0.5735	0.7362	1.4418	0.5727	0.6214	0.6292
ABD	0.6645	0.6911	0.6960	2.9927	3.6481	7.0181	0.7886	1.0034	2.5904	0.5685	0.6067	0.6146
Keep the core-ABD	0.6661	0.6994	0.7005	2.9835	3.2948	5.1622	0.7651	0.9787	1.7128	0.5699	0.6187	0.6257

Table 8. Quantitative comparison of different methods under the same backbone(SwinUNet) on the OASIS-1 and MRBrainS13 test sets. In the table, the best-performing metrics of our method and its corresponding baseline are highlighted in bold.

Model	Acc \uparrow			Pre \uparrow			Sen \uparrow			Spe \uparrow		
	CSF	GM	WM									
OASIS-1 dataset												
SwinUNet	0.9733	0.9659	0.9853	0.9176	0.9168	0.9338	0.8968	0.9159	0.9244	0.9780	0.9716	0.9890
Gaussian noise	0.9731	0.9653	0.9849	0.9154	0.9128	0.9350	0.8969	0.9165	0.9196	0.9778	0.9707	0.9892
Keep the core-Gaussian noise	0.9733	0.9657	0.9850	0.9157	0.9130	0.9354	0.8969	0.9166	0.9197	0.9810	0.9710	0.9893
Gaussian blur	0.9735	0.9660	0.9852	0.9115	0.9151	0.9389	0.9071	0.9189	0.9181	0.9776	0.9712	0.9895
Keep the core-Gaussian blur	0.9738	0.9671	0.9855	0.9117	0.9152	0.9389	0.9075	0.9192	0.9188	0.9777	0.9717	0.9897
Gamma	0.9726	0.9643	0.9845	0.9254	0.9065	0.9304	0.8777	0.9179	0.9192	0.9787	0.9695	0.9883
Keep the core-Gamma	0.9728	0.9645	0.9846	0.9255	0.9067	0.9307	0.8779	0.9181	0.9194	0.9789	0.9697	0.9887
Brightness contrast	0.9731	0.9656	0.9851	0.9192	0.9117	0.9361	0.8951	0.9184	0.9179	0.9780	0.9706	0.9892
Keep the core-Brightness contrast	0.9733	0.9657	0.9855	0.9195	0.9118	0.9366	0.8954	0.9189	0.9183	0.9781	0.9707	0.9895
Bias fields	0.9733	0.9659	0.9844	0.9204	0.9121	0.9437	0.8996	0.9236	0.9107	0.9781	0.9703	0.9887
Keep the core-Bias fields	0.9738	0.9663	0.9847	0.9207	0.9129	0.9443	0.8999	0.9241	0.9108	0.9786	0.9711	0.9884
Random Erasing	0.9723	0.9643	0.9843	0.9117	0.9029	0.9264	0.8908	0.9114	0.9205	0.9773	0.9703	0.9885
Keep the core-RandomErasing	0.9729	0.9648	0.9848	0.9176	0.9124	0.9274	0.8931	0.9154	0.9269	0.9780	0.9705	0.9886
Cutout	0.9732	0.9656	0.9851	0.9124	0.9123	0.9336	0.9014	0.9190	0.9218	0.9777	0.9709	0.9891
Keep the core-Cutout	0.9736	0.9661	0.9854	0.9126	0.9123	0.9337	0.9017	0.9198	0.9223	0.9779	0.9711	0.9896
Mixup	0.9726	0.9650	0.9852	0.9259	0.9165	0.9194	0.8796	0.9114	0.9376	0.9783	0.9707	0.9882
Keep the core-Mixup	0.9727	0.9658	0.9854	0.9263	0.9169	0.9203	0.8801	0.9117	0.9378	0.9788	0.9717	0.9883
Cutmix	0.9732	0.9658	0.9857	0.9209	0.9169	0.9422	0.9029	0.9229	0.9227	0.9775	0.9705	0.9896
Keep the core-Cutmix	0.9736	0.9659	0.9864	0.9231	0.9177	0.9432	0.9035	0.9230	0.9229	0.9778	0.9718	0.9899
HSMix	0.9731	0.9645	0.9845	0.9109	0.9158	0.9351	0.9072	0.9114	0.9169	0.9771	0.9701	0.9893
Keep the core-HSMix	0.9734	0.9647	0.9846	0.9116	0.9162	0.9352	0.9079	0.9118	0.9168	0.9777	0.9704	0.9895
MRS	0.9725	0.9655	0.9857	0.9184	0.9160	0.9427	0.9024	0.9229	0.9194	0.9768	0.9700	0.9900
Keep the core-MRS	0.9726	0.9655	0.9858	0.9186	0.9171	0.9428	0.9027	0.9233	0.9194	0.9769	0.9704	0.9902
ABD	0.9730	0.9655	0.9853	0.9147	0.9146	0.9386	0.8991	0.9186	0.9200	0.9775	0.9706	0.9897
Keep the core-ABD	0.9735	0.9656	0.9853	0.9152	0.9148	0.9395	0.8999	0.9187	0.9224	0.9777	0.9711	0.9898
MRBrainS13 dataset												
SwinUNet	0.7928	0.7912	0.9055	0.6766	0.6943	0.7338	0.6617	0.7085	0.7266	0.8025	0.7987	0.9107
Gaussian noise	0.7919	0.7903	0.8743	0.6688	0.6871	0.7254	0.6586	0.7003	0.6995	0.8020	0.7990	0.8796
Keep the core-Gaussian noise	0.7927	0.7909	0.8848	0.6751	0.6982	0.7258	0.6669	0.7072	0.7114	0.8022	0.8002	0.8896
Gaussian blur	0.7922	0.7910	0.9056	0.6726	0.6940	0.7271	0.6605	0.6987	0.6974	0.8022	0.7997	0.9107
Keep the core-Gaussian blur	0.7929	0.7916	0.9057	0.6755	0.6945	0.7276	0.6670	0.7030	0.6975	0.8024	0.7999	0.9109
Gamma	0.7926	0.7917	0.9164	0.6743	0.6987	0.7253	0.6650	0.7048	0.7214	0.8022	0.7998	0.9206
Keep the core-Gamma	0.7927	0.7928	0.9168	0.6756	0.6996	0.7243	0.6662	0.7055	0.7271	0.8023	0.7999	0.9207
Brightness contrast	0.7915	0.7898	0.9152	0.6554	0.6759	0.7300	0.6576	0.7020	0.7175	0.8012	0.7979	0.9211
Keep the core-Brightness contrast	0.7930	0.7914	0.9154	0.6834	0.6939	0.7378	0.6579	0.7142	0.7178	0.8031	0.7992	0.9297
Bias fields	0.7913	0.7900	0.9049	0.6646	0.6929	0.7284	0.6574	0.6955	0.6868	0.8013	0.7994	0.9109
Keep the core-Bias fields	0.7922	0.7996	0.9047	0.6736	0.6991	0.7120	0.6581	0.6971	0.6905	0.8022	0.7999	0.9111
Random Erasing	0.7898	0.7783	0.9154	0.6556	0.6733	0.7150	0.6368	0.6887	0.7025	0.8009	0.7878	0.9205
Keep the core-RandomErasing	0.7905	0.7893	0.9154	0.6569	0.6769	0.7227	0.6567	0.7100	0.7084	0.8015	0.7972	0.9211
Cutout	0.7930	0.7915	0.8639	0.6801	0.6952	0.7075	0.6648	0.7085	0.6916	0.8026	0.7997	0.8689
Keep the core-Cutout	0.7932	0.7922	0.9050	0.6817	0.6998	0.7136	0.6658	0.7093	0.7030	0.8031	0.7999	0.9103
Mixup	0.7911	0.7906	0.8640	0.6608	0.6934	0.7321	0.6571	0.6979	0.6685	0.8010	0.7998	0.8692
Keep the core-Mixup	0.7913	0.7909	0.8743	0.6605	0.6982	0.7382	0.6620	0.6992	0.6849	0.8017	0.8001	0.8794
Cutmix	0.7922	0.7905	0.9054	0.6725	0.6858	0.7407	0.6616	0.7130	0.6986	0.8021	0.7985	0.9106
Keep the core-Cutmix	0.7936	0.7918	0.9062	0.6839	0.6894	0.7465	0.6693	0.7246	0.7154	0.8031	0.7986	0.9114
HSMix	0.7919	0.7901	0.8740	0.6592	0.6933	0.7187	0.6765	0.7001	0.7024	0.8005	0.7989	0.8792
Keep the core-HSMix	0.7941	0.7924	0.8749	0.6858	0.6960	0.7325	0.6766	0.7203	0.7140	0.8030	0.7998	0.8796
MRS	0.7923	0.7911	0.8850	0.6766	0.6861	0.7251	0.6732	0.7139	0.7071	0.8023	0.7990	0.9000
Keep the core-MRS	0.7928	0.7915	0.8851	0.6799	0.6941	0.7312	0.6606	0.7142	0.7074	0.8029	0.7994	0.8900
ABD	0.7925	0.7903	0.8942	0.6731	0.6923	0.7161	0.6597	0.6976	0.6910	0.8021	0.7993	0.8895
Keep the core-ABD	0.7924	0.7910	0.8949	0.6746	0.6958	0.7163	0.6624	0.7092	0.7165	0.8023	0.7994	0.8896

Table 9. Quantitative comparison of different methods built on the same backbone (SwinUMamba, SOTA) on the OASIS-1 and MR-BrainS13 test sets. In the table, the best-performing metrics of our method and its corresponding baseline are highlighted in bold.

Model	Dice \uparrow			HD95(mm) \downarrow			ASD(mm) \downarrow			IOU \uparrow		
	CSF	GM	WM	CSF	GM	WM	CSF	GM	WM	CSF	GM	WM
OASIS-1 dataset												
SwinUMamba	0.9207	0.9261	0.9336	1.0219	1.0675	1.5723	0.1999	0.2471	0.3405	0.8688	0.8822	0.8938
Gaussian noise	0.9209	0.9267	0.9350	1.0188	1.0533	1.5169	0.2115	0.2476	0.3446	0.8696	0.8831	0.8957
Keep the core-Gaussian noise	0.9224	0.9269	0.9355	1.0117	1.0530	1.5088	0.2046	0.2469	0.3401	0.8720	0.8834	0.8960
Gaussian blur	0.9201	0.9251	0.9340	1.0373	1.0745	1.5269	0.2245	0.2496	0.3482	0.8688	0.8821	0.8944
Keep the core-Gaussian blur	0.9202	0.9257	0.9351	1.0369	1.0742	1.5209	0.2167	0.2466	0.3379	0.8692	0.8822	0.8962
Gamma	0.9195	0.9258	0.9352	1.0280	1.0719	1.5329	0.2031	0.2485	0.3591	0.8675	0.8819	0.8957
Keep the core-Gamma	0.9199	0.9265	0.9362	1.0276	1.0772	1.5325	0.2030	0.2405	0.3467	0.8680	0.8828	0.8961
Brightness contrast	0.9207	0.9270	0.9358	1.0173	1.0645	1.4700	0.2029	0.2473	0.3330	0.8690	0.8832	0.8962
Keep the core-Brightness contrast	0.9208	0.9275	0.9361	1.0230	1.0600	1.4653	0.2018	0.2438	0.3327	0.8691	0.8835	0.8964
Bias filesd	0.9198	0.9251	0.9337	1.0357	1.0776	1.5794	0.2090	0.2514	0.3554	0.8680	0.8806	0.8938
Keep the core-Bias filesd	0.9208	0.9263	0.9341	1.0212	1.0629	1.5118	0.2046	0.2469	0.3402	0.8685	0.8823	0.8945
Random Erasing	0.9174	0.9226	0.9290	1.0446	1.1222	1.7020	0.2301	0.2715	0.3918	0.8630	0.8756	0.8856
Keep the core-RandomErasing	0.9208	0.9264	0.9344	1.0218	1.0567	1.5434	0.2075	0.2534	0.3403	0.8693	0.8831	0.8945
Cutout	0.9229	0.9274	0.9341	1.0162	1.0769	1.5347	0.1994	0.2443	0.3211	0.8721	0.8843	0.8948
Keep the core-Cutout	0.9262	0.9275	0.9350	1.0161	1.0619	1.4930	0.2051	0.2366	0.3188	0.8785	0.8847	0.8954
Mixup	0.9223	0.9310	0.9367	1.0480	1.1090	1.6076	0.1966	0.2346	0.3553	0.8727	0.8908	0.9000
Keep the core-Mixup	0.9228	0.9314	0.9369	1.0479	1.1079	1.6070	0.1965	0.2342	0.3530	0.8730	0.8996	0.9040
Cutmix	0.9225	0.9287	0.9361	1.0435	1.1874	1.5402	0.1981	0.2383	0.3184	0.8723	0.8862	0.8980
Keep the core-Cutmix	0.9226	0.9288	0.9369	1.0406	1.1011	1.5377	0.1974	0.2354	0.3143	0.8704	0.8868	0.8992
HSMix	0.9245	0.9290	0.9360	1.0427	1.0958	1.5925	0.1918	0.2382	0.3582	0.8759	0.8871	0.8980
Keep the core-HSMix	0.9246	0.9291	0.9361	1.0424	1.0912	1.5923	0.1916	0.2370	0.3573	0.8769	0.8877	0.8981
MRS	0.9226	0.9292	0.9349	1.0389	1.0781	1.6082	0.1899	0.2379	0.3555	0.8731	0.8876	0.8966
Keep the core-MRS	0.9241	0.9300	0.9373	1.0388	1.0771	1.5714	0.1895	0.2354	0.3425	0.8756	0.8887	0.9001
ABD	0.9233	0.9276	0.9362	1.0215	1.0591	1.5057	0.1997	0.2450	0.3426	0.8731	0.8843	0.8972
Keep the core-ABD	0.9234	0.9273	0.9363	1.0218	1.0590	1.4861	0.1996	0.2449	0.3352	0.8739	0.8846	0.8976
MRBrainS13 dataset												
SwinUMamba	0.6855	0.7007	0.7017	1.9931	3.1604	7.2391	0.5097	0.9757	2.9280	0.5971	0.6211	0.6226
Gaussian noise	0.6795	0.6961	0.6887	2.0822	2.3922	6.4770	0.5551	0.6291	1.7222	0.5882	0.6118	0.6071
Keep the core-Gaussian noise	0.7031	0.7220	0.7266	1.6758	1.4775	3.4746	0.4438	0.4068	1.2211	0.6229	0.6515	0.6574
Gaussian blur	0.6860	0.7014	0.7289	1.8021	2.7995	6.0411	0.5266	0.7533	1.9572	0.5975	0.6218	0.6459
Keep the core-Gaussian blur	0.7042	0.7217	0.7437	1.6785	1.5229	3.0746	0.4249	0.3885	0.6557	0.6245	0.6513	0.6707
Gamma	0.6818	0.6973	0.6920	2.0986	3.2714	7.1900	0.5739	0.9384	2.7682	0.5921	0.6188	0.6159
Keep the core-Gamma	0.7013	0.7221	0.7416	1.8082	1.5780	2.9205	0.4293	0.4013	0.8358	0.6204	0.6516	0.6719
Brightness contrast	0.6777	0.6929	0.6648	2.1392	3.1398	9.0860	0.5138	0.8018	3.1472	0.5872	0.6100	0.5855
Keep the core-Brightness contrast	0.7038	0.7207	0.7429	1.6660	1.5377	3.0148	0.4335	0.4046	1.1556	0.6237	0.6497	0.6715
Bias filesd	0.6844	0.6995	0.7233	2.0534	3.1019	5.2166	0.5317	0.8232	1.9217	0.5956	0.6218	0.6465
Keep the core-Bias filesd	0.7034	0.7214	0.7525	1.6955	1.5451	3.7876	0.4291	0.3981	1.1525	0.6234	0.6510	0.6780
Random Erasing	0.6846	0.7023	0.6997	1.9876	3.0935	6.9380	0.5129	0.9197	3.1028	0.5960	0.6237	0.6239
Keep the core-RandomErasing	0.6999	0.7163	0.7392	1.7354	1.6958	3.9024	0.4512	0.4339	1.3344	0.6180	0.6425	0.6624
Cutout	0.6795	0.7000	0.6932	2.1639	3.2561	7.2707	0.5518	1.0129	3.0569	0.5890	0.6204	0.6124
Keep the core-Cutout	0.7024	0.7183	0.7369	1.6590	1.6520	3.7483	0.4404	0.4769	1.1730	0.6218	0.6456	0.6597
Mixup	0.6913	0.7090	0.7126	1.8336	2.2244	3.6060	0.5090	0.6094	1.0710	0.6049	0.6316	0.6349
Keep the core-Mixup	0.7033	0.7199	0.7353	1.8056	1.6822	3.8079	0.4312	0.3883	1.0967	0.6230	0.6486	0.6632
Cutmix	0.6808	0.6910	0.7042	2.0764	3.4679	7.3949	0.5312	0.9627	2.7047	0.5925	0.6074	0.6237
Keep the core-Cutmix	0.6967	0.7130	0.7121	1.9184	2.8017	4.0857	0.4494	0.7503	1.0156	0.6136	0.6398	0.6432
HSMix	0.6969	0.7122	0.7309	1.6475	1.6763	3.7915	0.4793	0.4734	0.8304	0.6137	0.6366	0.6531
Keep the core-HSMix	0.6996	0.7178	0.7319	1.8100	2.0304	3.6599	0.4532	0.4669	1.2284	0.6175	0.6457	0.6574
MRS	0.6864	0.7068	0.7103	2.0022	2.4285	5.0634	0.4859	0.6938	1.8649	0.5981	0.6312	0.6368
Keep the core-MRS	0.7024	0.7207	0.7249	1.7568	1.5814	3.3757	0.4250	0.4365	0.7065	0.6218	0.6499	0.6556
ABD	0.6835	0.6993	0.6976	2.0116	3.0385	7.3340	0.5784	0.8242	3.0102	0.5948	0.6181	0.6189
Keep the core-ABD	0.7041	0.7211	0.7381	1.6842	1.5596	2.6655	0.4211	0.4064	0.4790	0.6242	0.6501	0.6694

Table 10. Quantitative comparison of different methods built on the same backbone (SwinUMamba, SOTA) on the OASIS-1 and MR-BrainS13 test sets. In the table, the best-performing metrics of our method and its corresponding baseline are highlighted in bold.

Model	Acc↑			Pre↑			Sen↑			Spe↑		
	CSF	GM	WM									
OASIS-1 dataset												
SwinUMamba	0.9746	0.9684	0.9866	0.9334	0.9241	0.9509	0.9098	0.9299	0.9282	0.9785	0.9722	0.9899
Gaussian noise	0.9736	0.9676	0.9862	0.9256	0.9240	0.9496	0.9173	0.9301	0.9315	0.9771	0.9716	0.9893
Keep the core-Gaussian noise	0.9747	0.9686	0.9866	0.9289	0.9253	0.9493	0.9176	0.9302	0.9329	0.9782	0.9726	0.9898
Gaussian blur	0.9731	0.9680	0.9861	0.9297	0.9251	0.9489	0.9124	0.9271	0.9307	0.9769	0.9721	0.9893
Keep the core-Gaussian blur	0.9735	0.9682	0.9865	0.9260	0.9262	0.9505	0.9166	0.9274	0.9313	0.9770	0.9723	0.9896
Gamma	0.9736	0.9676	0.9868	0.9310	0.9248	0.9491	0.9099	0.9292	0.9328	0.9774	0.9715	0.9900
Keep the core-Gamma	0.9741	0.9681	0.9869	0.9321	0.9253	0.9497	0.9115	0.9295	0.9329	0.9778	0.9722	0.9901
Brightness contrast	0.9739	0.9682	0.9867	0.9304	0.9257	0.9517	0.9124	0.9298	0.9306	0.9776	0.9722	0.9900
Keep the core-Brightness contrast	0.9739	0.9688	0.9869	0.9319	0.9260	0.9520	0.9128	0.9299	0.9318	0.9772	0.9727	0.9900
Bias fields	0.9737	0.9674	0.9862	0.9289	0.9244	0.9482	0.9127	0.9273	0.9307	0.9774	0.9716	0.9894
Keep the core-Bias fields	0.9749	0.9685	0.9869	0.9290	0.9254	0.9498	0.9131	0.9277	0.9295	0.9776	0.9730	0.9895
Random Erasing	0.9744	0.9685	0.9864	0.9252	0.9237	0.9426	0.9119	0.9243	0.9277	0.9782	0.9730	0.9896
Keep the core-RandomErasing	0.9756	0.9686	0.9867	0.9277	0.9258	0.9482	0.9145	0.9265	0.9288	0.9798	0.9764	0.9898
Cutout	0.9746	0.9693	0.9857	0.9299	0.9242	0.9524	0.9170	0.9322	0.9268	0.9782	0.9729	0.9889
Keep the core-Cutout	0.9756	0.9699	0.9863	0.9356	0.9248	0.9506	0.9185	0.9332	0.9305	0.9786	0.9734	0.9896
Mixup	0.9743	0.9696	0.9874	0.9348	0.9323	0.9486	0.9123	0.9320	0.9375	0.9780	0.9733	0.9903
Keep the core-Mixup	0.9749	0.9700	0.9875	0.9347	0.9334	0.9491	0.9133	0.9330	0.9376	0.9786	0.9740	0.9905
Cutmix	0.9744	0.9688	0.9851	0.9310	0.9299	0.9502	0.9159	0.9294	0.9327	0.9778	0.9730	0.9881
Keep the core-Cutmix	0.9746	0.9688	0.9858	0.9335	0.9302	0.9519	0.9162	0.9300	0.9328	0.9780	0.9736	0.9888
HSMix	0.9746	0.9690	0.9868	0.9337	0.9300	0.9463	0.9173	0.9305	0.9377	0.9781	0.9730	0.9897
Keep the core-HSMix	0.9752	0.9696	0.9869	0.9338	0.9304	0.9468	0.9175	0.9309	0.9379	0.9887	0.9736	0.9899
MRS	0.9740	0.9685	0.9865	0.9351	0.9264	0.9512	0.9116	0.9337	0.9304	0.9777	0.9723	0.9895
Keep the core-MRS	0.9746	0.9693	0.9873	0.9355	0.9281	0.9515	0.9148	0.9339	0.9349	0.9782	0.9727	0.9904
ABD	0.9746	0.9687	0.9866	0.9289	0.9258	0.9506	0.9190	0.9310	0.9323	0.9780	0.9727	0.9897
Keep the core-ABD	0.9748	0.9689	0.9869	0.9293	0.9259	0.9515	0.9198	0.9388	0.9325	0.9787	0.9730	0.9899
MRBrainS13 dataset												
SwinUMamba	0.7949	0.7912	0.9159	0.6870	0.6854	0.7483	0.6877	0.7215	0.6981	0.8031	0.7986	0.9222
Gaussian noise	0.7937	0.7905	0.9053	0.6696	0.6938	0.7529	0.6937	0.7015	0.6548	0.8012	0.7998	0.9122
Keep the core-Gaussian noise	0.7973	0.7953	0.8661	0.6994	0.7123	0.7634	0.7089	0.7333	0.7059	0.8038	0.8019	0.8713
Gaussian blur	0.7947	0.7920	0.9267	0.6788	0.6937	0.7498	0.6965	0.7121	0.7324	0.8022	0.7998	0.9323
Keep the core-Gaussian blur	0.7975	0.7953	0.8869	0.7012	0.7165	0.7763	0.7088	0.7280	0.7301	0.8041	0.8022	0.8915
Gamma	0.7973	0.7952	0.8662	0.7086	0.7114	0.7643	0.6961	0.7346	0.7311	0.8048	0.8014	0.8705
Keep the core-Gamma	0.7937	0.7905	0.9053	0.6696	0.6938	0.7529	0.6937	0.7015	0.6548	0.8012	0.7998	0.9122
Brightness contrast	0.7946	0.7900	0.9045	0.6986	0.6779	0.7434	0.6653	0.7161	0.6337	0.8043	0.7973	0.9120
Keep the core-Brightness contrast	0.7973	0.7952	0.8767	0.6962	0.7157	0.7778	0.7131	0.7268	0.7230	0.8035	0.8023	0.8815
Bias fields	0.7944	0.7924	0.9057	0.6832	0.7000	0.7151	0.6919	0.7035	0.7758	0.8024	0.8008	0.9093
Keep the core-Bias fields	0.7974	0.7954	0.9183	0.7010	0.7144	0.7984	0.7080	0.7294	0.7358	0.8040	0.8022	0.9229
Random Erasing	0.7949	0.7916	0.9163	0.6904	0.6917	0.7341	0.6825	0.7187	0.7069	0.8035	0.7992	0.9212
Keep the core-RandomErasing	0.7966	0.7941	0.8967	0.6890	0.7107	0.7807	0.7129	0.7236	0.7185	0.8027	0.8017	0.9023
Cutout	0.7940	0.7908	0.9158	0.6811	0.6818	0.7441	0.6839	0.7254	0.6946	0.8027	0.7977	0.9219
Keep the core-Cutout	0.7971	0.7944	0.8865	0.6970	0.7069	0.7954	0.7093	0.7317	0.7036	0.8036	0.8011	0.8922
Mixup	0.7956	0.7930	0.8752	0.6869	0.6993	0.7488	0.6977	0.7217	0.6922	0.8031	0.8003	0.8809
Keep the core-Mixup	0.7972	0.7952	0.8868	0.6935	0.7193	0.7695	0.7150	0.7218	0.7190	0.8032	0.8028	0.8915
Cutmix	0.7947	0.7901	0.9155	0.6819	0.6949	0.7283	0.6863	0.6969	0.7050	0.8027	0.7995	0.9211
Keep the core-Cutmix	0.7966	0.7936	0.8653	0.7009	0.7000	0.7496	0.6961	0.7309	0.7097	0.8041	0.8005	0.8695
HSMix	0.7964	0.7940	0.9070	0.6869	0.7084	0.7887	0.7095	0.7100	0.7070	0.8027	0.8016	0.9129
Keep the core-HSMix	0.7968	0.7946	0.9071	0.6958	0.7094	0.7680	0.7165	0.7284	0.7225	0.8036	0.8018	0.9121
MRS	0.7952	0.7927	0.8960	0.6965	0.6943	0.7586	0.6801	0.7241	0.6975	0.8041	0.7994	0.9015
Keep the core-MRS	0.7972	0.7951	0.8660	0.7010	0.7130	0.7693	0.7058	0.7305	0.7093	0.8040	0.8022	0.8704
ABD	0.7940	0.7916	0.9056	0.6634	0.6951	0.7556	0.7103	0.7076	0.6817	0.8003	0.8000	0.9123
Keep the core-ABD	0.7975	0.7953	0.8663	0.7030	0.7147	0.7915	0.7167	0.7285	0.7235	0.8042	0.8021	0.8709

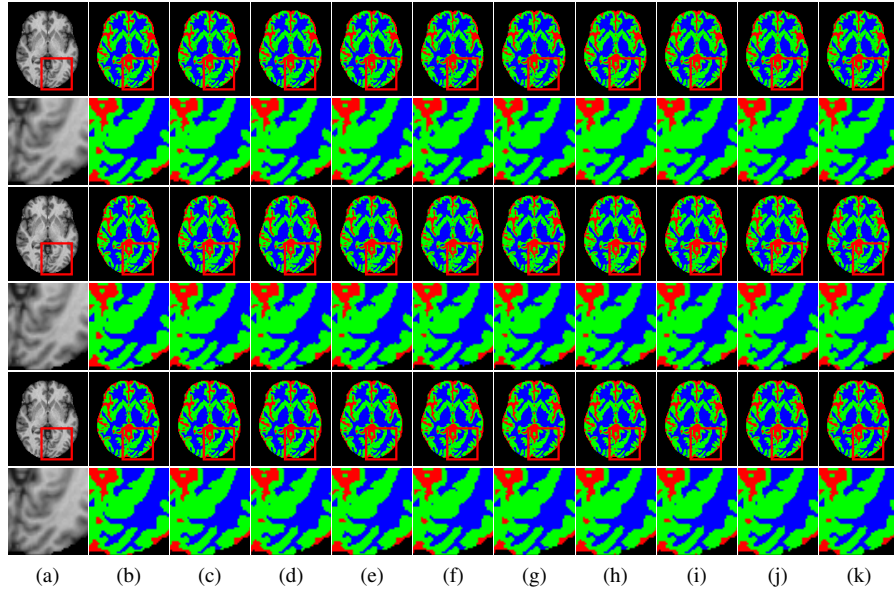


Figure 7. Comparison of segmentation results on the OASIS-1 dataset under different combinations of models and augmentation strategies. From top to bottom, the rows correspond to UNet, SwinUNet, and SwinUMamba. (a) Image, (b) GT, (c) Pred, (d) Gaussian noise, (e) Ours+Gaussian noise, (f) Mixup, (g) Ours+Mixup, (h) Cutmix, (i) Ours+Cutmix, (j) MRS(label), (k) Ours+MRS(label).

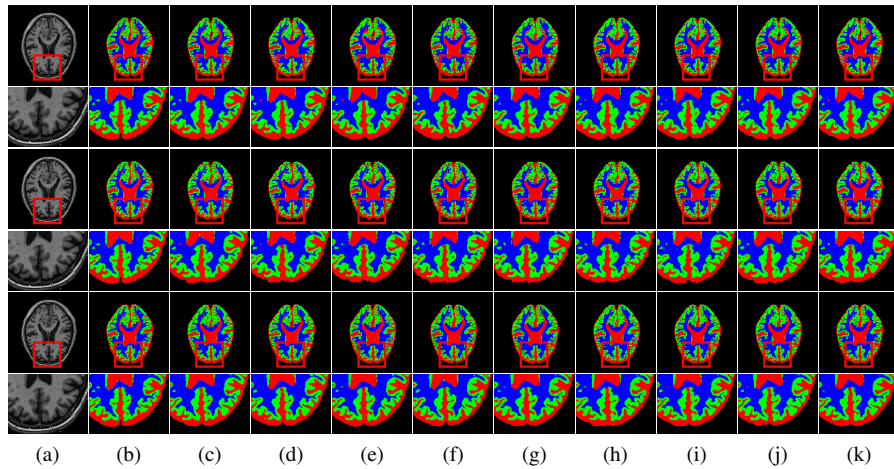


Figure 8. Comparison of segmentation results on the MRBrainS13 dataset under different combinations of models and augmentation strategies. From top to bottom, the rows correspond to UNet, SwinUNet, and SwinUMamba. (a) Image, (b) GT, (c) Pred, (d) Gaussian noise, (e) Ours+Gaussian noise, (f) Mixup, (g) Ours+Mixup, (h) Cutmix, (i) Ours+Cutmix, (j) MRS(label), (k) Ours+MRS(label).

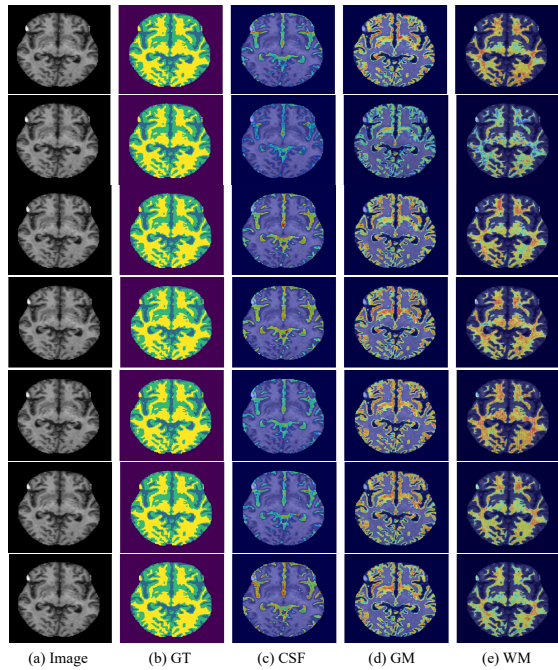


Figure 9. Class activation mapping (CAM) visualizations of different augmentation strategies on the OASIS-1 dataset. From top to bottom, the rows correspond to: Baseline, Random Erasing, Ours + Random Erasing, Cutout, Ours + Cutout, ABD (label), and Ours + ABD (label).

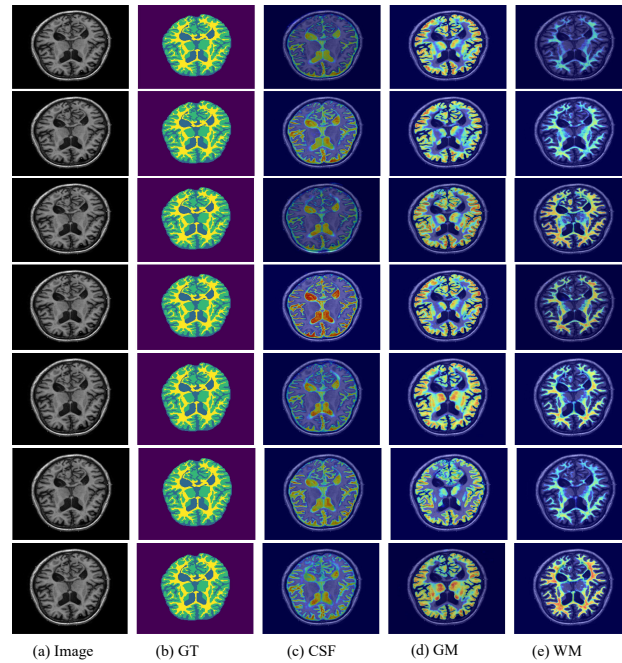


Figure 10. Class activation mapping (CAM) visualizations of different augmentation strategies on the MRBrainS13 dataset. From top to bottom, the rows correspond to: Baseline, Random Erasing, Ours + Random Erasing, Cutout, Ours + Cutout, ABD (label), and Ours + ABD (label).

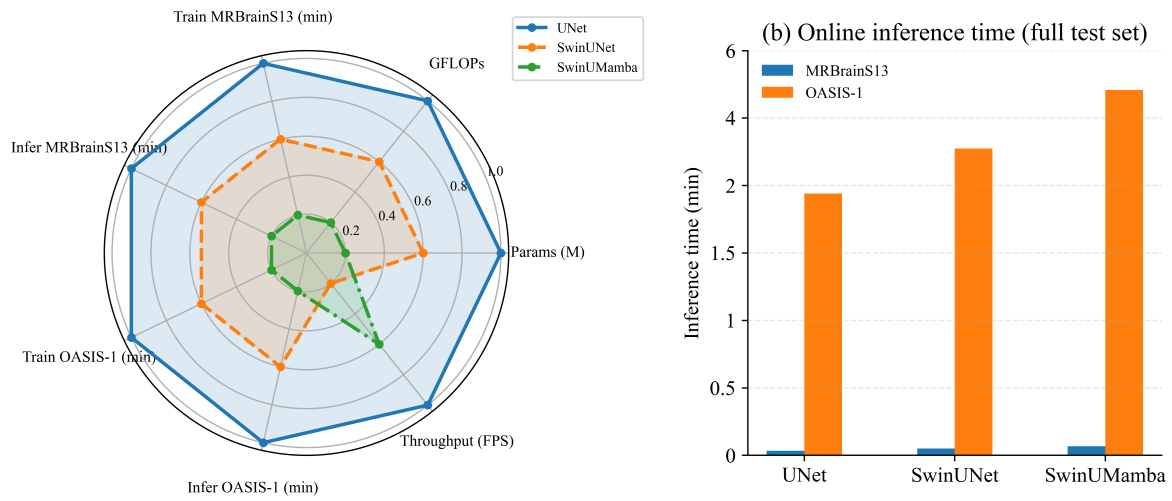


Figure 11. Computation cost across models, datasets, and online stages. (a) Normalized computation and throughput comparison across UNet, SwinUNet, and SwinUMamba, considering model size, FLOPs, training times, inference times, and throughput. (b) Online inference time on the full test sets for MRBrainS13 and OASIS-1.